Swarm Learning as a privacy-preserving machine learning approach for disease classification

Stefanie Warnat-Herresthal[1,*], Hartmut Schultze[2,*], Krishnaprasad Lingadahalli Shastry[2,*], Sathyanarayanan Manamohan[2], Saikat Mukherjee[2], Vishesh Garg[2], Ravi Sarveswara[2], Kristian Händler[3,*], Peter Pickkers[4,*], N. Ahmad Aziz[5,6,*], Sofia Ktena[7,*] Christian Siever[2], Michael Kraut[3], Milind Desai[2], Bruno Monnet[2], Maria Saridaki[7], Charles Martin Siegel[2], Anna Drews[3], Melanie Nuesch-Germano[1], Heidi Theis[3], Mihai G. Netea[8,9], Fabian Theis[10], Anna C. Aschenbrenner[1,8], Thomas Ulas[3], Monique M.B. Breteler[5,11,#], Evangelos J. Giamarellos-Bourboulis[7,#], Matthijs Kox[4,#], Matthias Becker[3,#], Sorin Cheran[2,#], Michael S. Woodacre[2,#], Eng Lim Goh[2,#], Joachim L. Schultze[1,3,#], German COVID-19 OMICS Initiative (DeCOI)

Affiliations:

1 Genomics and Immunoregulation, Life & Medical Sciences (LIMES) Institute, University of Bonn, 53115 Bonn, Germany
2 Hewlett Packard Enterprise
3 PRECISE Platform for Single Cell Genomics and Epigenomics, German Center for Neurodegenerative Diseases and the University of Bonn, 53127 Bonn, Germany
4 Department of Intensive Care Medicine and Radboud Center for Infectious Diseases (RCI), Radboud University Medical Center, Nijmegen, 6500HB, The Netherlands
5 Population Health Sciences, German Center for Neurodegenerative Diseases (DZNE), 53175 Bonn, Germany
6 Department of Neurology, Faculty of Medicine, University of Bonn, 53127 Bonn, Germany
7 4th Department of Internal Medicine, National and Kapodistrian University of Athens, Medical School, 124 62 Athens, Greece
8 Department of Internal Medicine and Radboud Center for Infectious Diseases (RCI), Radboud University Medical Center, Nijmegen 6500HB, The Netherlands
9 Immunology & Metabolism, Life and Medical Sciences (LIMES) Institute, University of Bonn, Bonn 53115, Germany
10 Institute of Computational Biology, Helmholtz Center Munich (HMGU), 85764 Neuherberg, Germany
11 Institute for Medical Biometry, Informatics and Epidemiology (IMBIE), Faculty of Medicine, University of Bonn, 53175 Bonn, Germany

* shared first authors
\# shared last authors
corresponding author j.schultze@uni-bonn.de

Key Words:

machine learning, artificial intelligence, Swarm Learning, decentralized machine learning, privacy preserving machine learning, transcriptomics, blood, blood transcriptomics, acute myeloid leukemia, acute lymphoblastic leukemia, COVID-19, tuberculosis

Abstract

Identification of patients with life-threatening diseases including leukemias or infections such as tuberculosis and COVID-19 is an important goal of precision medicine. We recently illustrated that leukemia patients are identified by machine learning (ML) based on their blood transcriptomes. However, there is an increasing divide between what is technically possible and what is allowed because of privacy legislation. To facilitate integration of any omics data from any data owner world-wide without violating privacy laws, we here introduce Swarm Learning (SL), a decentralized machine learning approach uniting edge computing, blockchain-based peer-to-peer networking and coordination as well as privacy protection without the need for a central coordinator thereby going beyond federated learning. Using more than 14,000 blood transcriptomes derived from over 100 individual studies with non-uniform distribution of cases and controls and significant study biases, we illustrate the feasibility of SL to develop disease classifiers based on distributed data for COVID-19, tuberculosis or leukemias that outperform those developed at individual sites. Still, SL completely protects local privacy regulations by design. We propose this approach to noticeably accelerate the introduction of precision medicine.

Introduction

Fast and reliable detection of patients with severe illnesses is a major goal of precision medicine[1]. The measurement of molecular phenotypes for example by omics technologies[2] and the application of sophisticated bioinformatics including artificial intelligence (AI) approaches[3–7] opens up the possibility for physicians to utilize large-scale data for diagnostic purposes in an unprecedented way. Yet, there is an increasing divide between what is technically possible and what is allowed because of privacy legislation[8] (hhs.gov, https://www.hhs.gov/hipaa/index.html, 2020; Intersoft Consulting, General Data Protection Regulation, https://gdpr-info.eu; Convention for the Protection of Individuals with regard to Automatic Processing of Personal Data, https://rm.coe.int/16808ade9d). Particularly, in a global health crisis, as in the case of the infection with severe acute respiratory syndrome coronavirus 2 (SARS-CoV-2) leading to the pandemic spread of coronavirus disease 2019 (COVID-19)[9–11], reliable, fast, secure and privacy-preserving technical solutions based on AI principles are now believed to add to the armamentarium to quickly answer important questions in the fight against such threats[12–15]. These AI-based concepts range from protein

structure prediction[16], drug target prediction[17], knowledge sharing[18], tools for population control[19,20] to the assistance of healthcare personnel, e.g. by developing AI-based coronavirus diagnostic software[21,22]. Considering the more clinically oriented AI-based technical solutions, any such progress might also induce improvements for a variety of deadly diseases including other major infections or cancer[23]. For example, the principles of a recently introduced AI-system for diagnosing COVID-19 pneumonia and predicting disease outcome using computed tomography[22] might be further developed to identify patients with tuberculosis or lung cancer in the future[24]. At the same time, we need to consider important standards relating to data privacy and protection, such as Convention 108(+) of the Council of Europe (Convention for the Protection of Individuals with regard to Automatic Processing of Personal Data, https://rm.coe.int/16808ade9d), which regulate the use and sharing of health data including in AI-based approaches, irrespective of the occurrence of a pandemic crisis.

AI-based solutions intrinsically rely on appropriate algorithms[25], but even more so on large enough datasets for training purposes[26]. Since the domain of medicine is inherently decentralized, the volume of data available locally is often insufficient to train reliable classifiers[27–29]. As a consequence, centralization of data, for example via cloud solutions, has been one model to address the local limitations[30–32]. While beneficial from an AI-perspective, centralized solutions were shown to have other inherent hurdles, including increased data traffic of large medical data, data ownership, privacy and security concerns when ownership is disconnected from access and usage curation and thereby creating data monopolies favoring data aggregators[26]. Consequently, solutions to the challenges of central data models in AI - particular when dealing with medical data - must be effective, with high accuracy and efficiency, privacy- and ethics-preserving, secure, and fault-tolerant by design[33–36]. Federated AI has been introduced to address some of these aspects[26,37–39]. While data are kept locally (at the edge) and privacy issues are addressed[40,41], the model parameters in federated AI are still handled by central custodians who as the intermediaries concentrate power of the learning to themselves. Furthermore, such star-shaped architectures decrease fault tolerance.

We hypothesized that completely decentralized AI solutions overcome current technical shortcomings and at the same time accommodate for inherently decentralized data structures in medicine as well as pronounced data privacy and security regulations. The solution would 1) need to keep large medical data locally with the data owner, 2) require no raw data exchange thereby also reducing data traffic and issues related to central storage, 3) provide high level data security and privacy protection, 4) guarantee secure, transparent and fair onboarding of decentralized members participating in the learning network without the need for a central custodian, 5) allow for parameter merging with equal rights for all members requiring no central custodian, and 6) protect the ML models from attacks. To address these

points, we introduce the concept of Swarm Learning (SL). SL combines decentralized hardware infrastructures, distributed ML technique based on standardized AI engines with a permissioned blockchain to securely onboard members, dynamically elect the leader among the members, and merge model parameters. All processes are orchestrated by an SL library and an iterative learning procedure applying AI solutions to compute problems with decentralized private data.

Medicine is a prime example to illustrate the advantages of this AI approach. Without any doubt, numerous medical features including radiograms or computed tomographies, proteomes, metagenomes or microbiomes derived from body fluids including nasal or throat swaps, blood, urine or stool are all excellently suitable medical data for the development of AI-based diagnostic or outcome prediction classifiers. We here chose to evaluate the cellular compartment of peripheral blood, either in form of peripheral blood mononuclear cells (PBMC) or whole blood-derived transcriptomes, since blood-derived transcriptomes include important information about the patients' immune response during a certain disease, which in itself is an important molecular information[42,43]. In other words, in addition to the use of blood-derived high-dimensional molecular features for a diagnostic or outcome classification problem, blood transcriptomes could be further utilized in the clinic to systematically characterize ongoing pathophysiology, predict patient-specific drug targets and trigger additional studies targeting defined cell types or molecular pathways, making this feature space even more attractive to answer a wide variety of medical questions. Here, we illustrate that newly generated blood transcriptome data together with data derived from more than 14,000 samples in more than 100 studies combined with AI-based algorithms in a Swarm Learning environment can be successfully applied in real-world scenarios to detect patients with leukemias, tuberculosis or active COVID-19 disease in an outbreak scenario across distributed datasets without the necessity to negotiate and contractualize data sharing.

Results

Concept of Swarm Learning

Machine learning (ML) of any data including genome or transcriptome data requires the availability of sufficiently large datasets[26,44] and the respective compute infrastructure including data storage for data processing and analytics[45]. Conceptually, if data and compute infrastructure is sufficiently available locally, ML can be performed locally ('at the edge') (**Fig. 1a**). However, often medical data are not sufficiently large enough locally and similar

153 approaches are performed at different locations in a disconnected fashion. These limitations
154 have been overcome by cloud computing where data are moved centrally to perform training
155 of ML algorithms in a centralized compute environment (**Fig. 1b**). Compared to local
156 approaches, cloud computing can significantly increase the amount of data for training ML
157 algorithms and therefore significantly improve their results[26]. However, cloud computing has
158 other disadvantages such as data duplication from local to central data storage, increased
159 data traffic and issues with locally differing data privacy and security regulations[46]. As an
160 alternative, federated cloud computing approaches such as Google's federated learning[38] and
161 Facebook's elastic averaging SGD (Deep learning with Elastic Averaging SGD,
162 http://papers.neurips.cc/paper/5761-deep-learning-with-elastic-averaging-sgd.pdf) have been
163 developed. In these models, dedicated parameter servers are responsible for aggregating and
164 distributing local learning (**Fig. 1c**). A disadvantage of such star-shaped system architectures
165 is the remainder of a central structure, which hampers implementation across different
166 jurisdictions and therefore still requires the respective legal negotiations. Furthermore, the risk
167 for a single point of failure at the central structure reduces fault-tolerance.

168 In an alternative model, which we introduce here as Swarm Learning (SL), we dismiss the
169 dedicated server and allow parameters and models to be shared only locally (**Fig. 1d**). While
170 parameters are shared via the swarm network, the models are built independently on private
171 data at the individual sites, here referred to as swarm edge nodes (short 'nodes') (**Fig. 1e**). SL
172 provides security measures to guarantee data sovereignty, security and privacy realized by a
173 private permissioned blockchain technology which enables different organizations or consortia
174 to efficiently collaborate (**Fig. 1f**). In a private permissioned blockchain network, each
175 participant is well defined and only pre-authorized participants can execute the transactions.
176 Hence, they use computationally inexpensive consensus algorithms, which offers better
177 performance and scalability. Onboarding of new members or nodes can be done dynamically
178 with the appropriate authorization measures to know the participants of the network, which
179 allows continuous scaling of learning (**Extended Data Fig. 1a**). A new node enrolls via a
180 blockchain smart contract, obtains the model, and performs local model training until defined
181 conditions for synchronization are met. Next, model parameters are exchanged via a Swarm
182 API with the rest of the swarm members and merged for an updated model with updated
183 parameter settings to start a new round of training at the nodes. This process is repeated until
184 stopping criterions are reached, which are negotiated between the swarm nodes/members.
185 The leader is dynamically elected using a blockchain smart contract for merging the
186 parameters and there is no need for a central coordinator in this swarm network. The
187 parameter merging algorithm is executed using a blockchain smart contract thus protects it
188 from semi-honest or dishonest participants. The parameters can be merged by the leader

using different functions including average, weighted average, minimum, maximum, or median functions. The various merge techniques and merge frequency enables SL to efficiently work with imbalanced and biased data. As currently developed, SL works with parametric models with finite sets of parameters, such as linear regression or neural network models.

At each node, SL is conceptually divided into infrastructure and application layer (**Fig. 1g**). On top of the physical infrastructure layer (hardware) the application environment contains the ML platform, the blockchain, and the SL library (SLL) including the Swarm API in a containerized deployment, which allows SL to be executed in heterogeneous hardware infrastructures (**Fig. 1g, Supplementary Information**). The application layer consists of the content, the models from the respective domain, here medicine (**Fig. 1g**), for example blood transcriptome data from patients with leukemias, tuberculosis and COVID-19 (**Fig. 1h-l**). Collectively, Swarm Learning allows for a completely decentralized and therefore democratized, secure, privacy-preserving, hardware-independent, and scalable machine learning environment, applicable to many scenarios and domains, which we demonstrate with three medical examples.

Swarm learning robustly predicts leukemias from peripheral blood mononuclear cell data

As a first use case, we chose transcriptomes derived from peripheral blood mononuclear cells (PBMC) of more than 12,000 individuals (**Fig. 1h-j**) separated into three individual datasets (A1, A2, A3) based on the technology used for generating the transcriptomes (2 different microarrays, RNA-seq)[47]. We used a deep neural network (Keras, https://keras.io/, 2015) as the machine learning approach in all three use cases. To assess performance metrics of SL, we simulated scenarios by dividing up the individual samples derived from several independently performed studies (see Material and Methods) within each of the three datasets into non-overlapping training and test sets. The training sets were then distributed to three nodes for training and classifiers were tested at a fourth node (independent test set) (**Fig. 2a**). By assigning the training data to the nodes in different distributions, we mimicked several clinically relevant scenarios (**Supplementary Table 1)**. As cases, we first used samples defined as acute myeloid leukemia (AML), all other samples are termed ‘controls’. Each node within this simulation could stand for a large hospital or center, a network of hospitals performing individual studies together, a country or any other independent institutional organization generating such medical data with local privacy requirements.

In a first scenario, we randomly distributed samples per node as well as cases and controls unevenly at the nodes and between nodes (dataset A2) (**Fig. 2b**). Sample distribution between sample sets was permuted 100 times (**Fig. 2b, middle panel**) to determine the influence of

individual samples on overall performance. Among the nodes, the best test results were obtained by node one with a mean accuracy of 97.0%, mean sensitivity of 97.5% and mean specificity of 96.3% with an even distribution between cases and controls, albeit this node had the smallest number of overall training samples. Node 2 did not produce any meaningful results, which was due to a too low ratio of cases to controls (1:99) for training. Surprisingly, node 3 with the largest number of samples, but an uneven distribution (70% cases : 30% controls) performed worse than node 1 with a mean balanced accuracy of 95.1%. Most importantly, however, SL outperformed each of the nodes resulting in a higher test accuracy in 97.0% of all permutations (mean balanced accuracy 97.7%) (**Fig. 2b, right panel, Supplementary Table 4**). The balanced accuracy of SL was significantly higher ($p < 0.001$) when compared to the performance of each of the three nodes, despite the fact that information from the poorly performing node 2 was integrated. We also calculated this scenario in datasets A1 and A3 and obtained rather similar results strongly supporting that the performance improvement of SL over single nodes is independent of data collection (studies) and even experimental technologies (microarray (datasets A1, A2), RNA-seq (dataset A3) used for data generation (**Extended Data Fig. 2**).

To test whether more evenly distributed samples at the nodes would improve individual node performance, we distributed similar numbers of samples to each of the nodes but kept case:control ratios as in scenario 1 (**Fig. 2c, Extended Data Fig. 3**). While there was a slight increase in test accuracy at nodes 1 and 2, node 3 performed worse with also higher variance. More importantly, SL still resulted in the best performance metrics (mean 98.5% accuracy) with slightly but significantly ($p<0.001$) increasing performance compared to the first scenario. Results derived from datasets A1 and A3 echoed these findings (**Extended Data Fig. 3**).

In a third scenario, we distributed the same number of samples across all three nodes, but increased potential batch effects between nodes, by distributing samples of a clinical study independently performed and published in the past only to a dedicated training node. In this scenario, cases and control ratios varied between nodes and left out samples (independent samples) from the same published studies were combined for testing at node 4. Performance of the three nodes was very comparable, but never reached SL results (mean 98.3% accuracy, swarm outperformed all nodes with $p<0.001$, **Fig. 2d., Extended Data Fig. 4b, Supplementary Data Table 4**), which was also true for datasets A1 and A3 (**Extended Data Fig. 4c-d**). Even when further increasing batch effects by distributing samples from independent published studies to the test node, which means that training and test datasets come from studies performed and published independently, SL outperformed the individual nodes, albeit the variance in the results was increased both at each node and for SL, indicating

259 that study design has an overall impact on classifier performance and that this is still seen in
260 SL (mean 95.6% accuracy, **Extended Data Fig. 4e**).

261 In a fourth scenario, we further optimized the nodes by increasing the overall sample size at
262 node 3 and keeping case:control ratios even at all nodes (**Fig. 2e, Extended Data Fig. 5a-d**).
263 Clearly, node performance further improved with little variance between permutations,
264 however, even under these 'node-optimized' conditions, SL led to higher performance
265 parameters.

266 In a fifth scenario, we tested whether or not SL was 'immune' against the impact of the data
267 generation procedure (microarray versus RNA-seq) (**Fig. 2f, Extended Data Fig. 5e,f**). We
268 recently demonstrated that classifiers trained on data derived by one technology (e.g.
269 microarrays) do not necessarily perform well on another (e.g. RNA-seq)[47]. To test this
270 influence on SL, we distributed the samples from the three different datasets (A1-A3) to one
271 node each, e.g. dataset A1 was used for training only at node 1. We used 20% of the data
272 (independent non-overlapping to the training data) from each dataset (A1-A3) and combined
273 them to form the test set (node 4). Node 3, trained on RNA-seq data, performed poorly on the
274 combined dataset due to the fact that two-thirds of the data in the test set were microarray-
275 derived data. Nodes 1 and 2 performed reasonably well with mean accuracies of 96.1% (node
276 1) and 97.5% (node 2), however did not reach the test accuracy of SL (98.8%), which also
277 indicated that SL is much more robust toward effects introduced by different data production
278 technologies in transcriptomics (**Fig. 2f, Extended Data Fig. 5e,f**).

279 Finally, we repeated several of these scenarios with acute lymphoblastic leukemia (ALL) as
280 the second most prevalent disease in dataset A2 (**Extended Data Fig. 6** and data not shown)
281 and demonstrated very similar results with SL outperforming the classifiers built at the nodes.
282 Collectively, these simulations using real-world transcriptome data collected from more than
283 100 individual studies illustrate that SL would not only allow data to be kept at the place of
284 generation and ownership, but it also outperforms every individual node in numerous
285 scenarios, even in those with nodes included that cannot provide any meaningful classifier
286 results.

287

288 **Swarm learning to identify patients with tuberculosis**

289 In infectious diseases, heterogeneity may be more pronounced compared to leukemia,
290 therefore we built a second use case predicting cases with tuberculosis (Tb) from full blood
291 transcriptomes. Of interest, previous work in smaller studies had already suggested that acute
292 tuberculosis or outcome of tuberculosis treatment can be revealed by blood transcriptomics

293 [48–52]. To apply SL, we generated a new dataset based on full blood transcriptomes derived by
294 PaxGene blood collection followed by bulk RNA-sequencing. We also generated new blood
295 transcriptomes and added existing studies to the dataset compiling a total of 1,999 samples
296 from nine individual studies including 775 acute and 277 latent Tb cases (**Fig. 1k, Extended**
297 **Data Fig. 7a, Supplementary Table 2**). These data are more challenging, since infectious
298 diseases show more variety due to biological differences with respect to disease severity,
299 phase of the disease or the host response. But also the technology itself is more variable with
300 numerous different approaches for full blood transcriptome sample processing, library
301 production and sequencing, which can introduce technical noise and batches between
302 studies. As a first scenario, we used all Tb samples (latent and acute) as cases and divided
303 Tb cases and controls evenly among the nodes (**Extended Data Fig. S7a-b, Supplementary**
304 **Table 1**). Similar to AML and ALL, in detecting Tb, SL outperformed the individual nodes in
305 accuracy (mean 93.4%), sensitivity (mean 96.0%) and specificity (mean 90.9%) (**Extended**
306 **Data Fig. S7b**). To increase the challenge, we decided to assess prediction of acute Tb cases
307 only. In this scenario, latent Tb are not treated as cases but rather as controls (**Extended Data**
308 **Fig. S7a**). For the first scenario, we kept cases and controls even at all nodes but further
309 reduced the number of training samples (**Fig. 3a-b**). As expected in this more challenging
310 scenario, distinguishing acute Tb from the control cohort (including latent Tb samples), overall
311 performance (mean balanced accuracy 89.1%, mean sensitivity 92.2%, mean specificity
312 86.0%) slightly dropped, but still SL performed better than any of the individual nodes ($p<0.01$
313 for swarm vs. each node, **Fig. 3b**). To determine whether sample size impacts on prediction
314 results in this scenario, we reduced the number of samples at each training node (1-3) by
315 50%, but kept the ratio between cases and controls (**Extended Data Fig. S7c**). Still, SL
316 outperformed the nodes, but all statistical readouts (mean accuracy 86.5%, mean sensitivity
317 87.8%, mean specificity 84.8%) at all nodes and SL showed lower performance, following
318 general observations of AI with better performance when increasing training data[26]. We next
319 altered the scenario by dividing up the three nodes into six smaller nodes (**Fig. 3c**, samples
320 per node reduced by half in comparison to **Fig. 3a-b**), a scenario that can be envisioned in the
321 domain of medicine in many settings, for example if several smaller medical centers with less
322 cases would join efforts (**Fig. 3d**). Clearly, each individual node performed worse, but for SL
323 the results did not deteriorate (mean accuracy 89.2%, mean sensitivity 90.7%, mean
324 specificity 88.2% with significant difference to each of the nodes in all performance measures,
325 see **Supplementary Table 4**), again illustrating the strength of the joined learning effort, while
326 completely respecting each individual node's data privacy.

327 Albeit aware of the fact that - in general - acute Tb is an endemic disease and does not tend
328 to develop towards a pandemic such as the current COVID-19 pandemics, we utilized the Tb

329 blood transcriptomics dataset to simulate potential outbreak and epidemic scenarios to
330 determine benefits, but also potential limitations of SL and how to address them (**Fig. 3e-l**).
331 The first scenario reflects a situation in which three independent regions (simulated by the
332 nodes), would already have sufficient but different numbers of disease cases. Furthermore,
333 cases and controls were kept even at the test node (**Fig. 3e-f**). Overall, compared to the
334 scenario described in **Fig. 3c**, results for the swarm were almost comparable (mean accuracy
335 89.0%, mean sensitivity 94.4%, mean specificity 83.4%), while the results for the node with
336 the lowest number of cases and controls (node 2) dropped noticeable (mean accuracy 82.2%,
337 mean sensitivity 88.8%, mean specificity 75.4%, **Fig. 3f**). When reducing the prevalence at
338 the test node by increasing the number of controls (**Fig. 3g-h**), this effect was even more
339 pronounced, while the performance of the swarm was almost unaffected (mean balanced
340 accuracy 89.0%).

341 We decreased the number of cases at a second training node (node 1) (**Fig. 3i-l**), which clearly
342 reduced test performance for this particular node (**Fig. 3i-j**), while test performance of the
343 swarm was only slightly inferior to the prior scenario (mean balanced accuracy 87.5%, no
344 significant difference to the prior scenario). Only when reducing the prevalence at the test
345 node (**Fig. 3k-l**), we saw a further drop in mean specificity for the swarm (81.0%), while
346 sensitivity stayed similarly high (93.0%). Finally, we further reduced the prevalence at two
347 training nodes (node 2: 1:10; node 3: 1:5) as well as the test node (**Extended Data Fig. 8a-**
348 **b**). Lowering the prevalence during training resulted in very poor test performance at these
349 two nodes (balanced accuracy node 2: 59.8%, balanced accuracy node 3: 74.8%), while
350 specificity was high (node 2: 98.4%, node 3: 93.8%). SL showed highest accuracy (mean
351 balanced accuracy 86.26%) and F-statistics (90.0%) but was outperformed for sensitivity by
352 node 1 (swarm: 80.0%, node1: 87.8%), which showed poor performance concerning
353 specificity (swarm: 92.4%, node1: 84.8%). Vice versa, node 2 outperformed the swarm for
354 specificity (98.4%), but showed very poor sensitivity (21.2%) (**Extended Data Fig. 8b**). When
355 lowering prevalence at the test node (**Extended Data Fig. 8c-d**), it became clear that all
356 performance parameters including the F1 statistics were more resistant for the swarm
357 compared to individual nodes. Taken together, using whole blood transcriptomes instead of
358 PBMC and acute Tb as the disease instead of leukemia, we present a second use case
359 illustrating that Swarm Learning integrating several individual nodes outperforms each node.
360 Furthermore, we gained initial insights into the potential of SL to be utilized in a disease
361 outbreak scenario.

362

363 **Identification of COVID-19 patients in an outbreak scenario**

364 Based on the promising results obtained for tuberculosis, we collected blood from COVID-19
365 patients at two sites in Europe (Athens, Greece; n=39 samples, Nijmegen, n=93 samples) and
366 generated whole blood transcriptomes by RNA-sequencing. We used the dataset described
367 for Tb as the framework and included the COVID-19 samples (**Fig. 1l**) for assessing whether
368 SL could be applied early on to detect patients with a newly identified disease. While COVID-
369 19 patients are currently identified by PCR-based assays to detect viral RNA[53], we use this
370 case as a proof-of-principle study to illustrate how SL could be used even very early on during
371 an outbreak based on the patients' immune response captured by analysis of the circulating
372 immune cells in the blood. Here, blood transcriptomes only present a potential feature space
373 to illustrate the performance of SL. Furthermore, assessing the specific host response, in
374 addition to disease prediction, might be beneficial in situations for which the pathogen is
375 unknown, specific pathogen tests not yet possible, and blood transcriptomics can contribute
376 to the understanding of the host's immune response[54]. Lastly, while we do not have the power
377 yet, blood transcriptome-based machine learning might be used to predict severe COVID-19
378 cases, which cannot be done by viral testing alone.

379 COVID-19 induces very strong changes in peripheral blood transcriptomes[54]. Following our
380 experience with the leukemia and tuberculosis use cases, we first tested classifier
381 performance for evenly distributed cases and controls at both training nodes and the test node
382 (**Extended Data Fig. 9a,b, Supplementary Table 1)**. We reached very high statistical
383 performance parameters, including high F1-statistics with SL showing highest mean values
384 for accuracy (96.4%), sensitivity (97.8%), and F1 score (96.4%) (**Extended Data Fig. 9b,**
385 summary statistics for all figures are listed in **Supplementary Table 4**). Reducing the
386 prevalence at the test node (11:25 cases:controls) reduced all test parameters (**Extended**
387 **Data Fig. 9c**), but only when we reduced the prevalence even further (1:44 ratio, **Extended**
388 **Data Fig. 9d**), F1-statistics was clearly reduced, albeit SL again performing best. We next
389 reduced the cases at all training nodes (**Extended Figure 10**), but even under these
390 conditions, we observed still very high values for accuracy, sensitivity, specificity and F1
391 scores, both derived by training at individual nodes or by SL (**Extended Figure 10a-f**).

392 We then reduced the cases at all three training nodes to very low numbers, a scenario that
393 might be envisioned very early during an outbreak scenario (**Fig. 4a**). Node 1 contained only
394 20 cases, node 2 10 cases and node 3 only 5 cases. At each node, controls outnumbered
395 cases by 1:5, 1:10, or 1:20. At the test node, we varied the prevalence from 1:1 (**Fig. 4b**), 1:2
396 (**Fig. 4c**) to 1:10 (**Fig. 4d**). Based on our findings for Tb (**Extended Data Fig. 8**), we expected
397 classifier performance to deteriorate under these conditions. We only observed decreased
398 performance at nodes 2 and 3 in these scenarios with SL outperforming these nodes with
399 $p<0.05$ for all performance measures, e.g. at a test node prevalence of 1:10 (accuracy

400 (99.3%), sensitivity (95.1%), specificity (99.7%) and F1-statistics (99.7%) (**Fig. 4d**). Finally,
401 we simulated a scenario with four instead of three training nodes with very few cases per node
402 (**Extended Data Fig. 11a-d**), in an otherwise similar scenario as described for Fig. 4. Even for
403 a simulated prevalence of 1:10 cases versus controls at the test node, we determined high
404 test performance parameters for SL, with swam performance being significantly higher than
405 node performances (SL accuracy (99.1%), sensitivity (92.0%), specificity (99.9%), F1 statistics
406 (99.7%) (**Extended Data Fig. 11**) with the lowest variance in performance, while results at
407 individual notes were very variable and deteriorated with low case numbers at the training
408 node. Collectively, we provide first evidence that blood transcriptomes taken from patients with
409 COVID-19 harbor very strong biological changes and these translate into a very powerful
410 feature space for applying machine learning to the detection of patients with this new infectious
411 disease, particularly when applying SL.

412

413 Discussion

414 The introduction of precision medicine based on high-resolution molecular and imaging data
415 will heavily rely on trustworthy machine learning algorithms in compute environments that are
416 characterized by high accuracy and efficiency, that are privacy- and ethics-preserving, secure,
417 and that are fault-tolerant by design[33–36]. At the same time, privacy legislation is becoming
418 increasingly strict, as risks of cloud-based and central data-acquisition are recognized. Here,
419 we introduce Swarm Learning, which combines blockchain technology and machine learning
420 environments organized in a swarm network architecture with independent swarm edge nodes
421 that harbor local data, compute infrastructure and execute the shared learning models that
422 make central data acquisition obsolete. During iterations of SL, one of the nodes is chosen to
423 lead the iteration, which does not require a central parameter server anymore thereby
424 restricting centralization of learned knowledge and at the same time increasing resiliency and
425 fault tolerance. In fact, these are the most important improvements over current federated
426 computing models. Furthermore, private permissioned blockchain technology, harboring all
427 rules of interaction between the nodes, is the Swarm Learning's inherent privacy- and ethics-
428 preserving strategy. This is of particular interest to medical data and could be adapted by other
429 federated learning systems. To understand whether the concept of swarm learning would also
430 be characterized by high efficiency and high accuracy, we built three medical use cases based
431 on blood transcriptome data, which are high-dimensional data derived from blood, one of the
432 major tissues used for diagnostic purposes in medicine. First, utilizing three previously
433 compiled datasets (A1-3) of peripheral blood mononuclear cells derived from patients with
434 acute myeloid leukemia, we provide strong evidence that SL-based classifier generation using

435 a well-established neural network algorithm outperforms individual nodes, even in scenarios
436 where individual contributing swarm nodes were performing rather poorly. Most striking,
437 swarm learning was even improving performance parameters when training of individual
438 nodes was based on technically different data, a situation that was previously shown to
439 deteriorate classifier performance[47]. With these promising results, we generated a more
440 challenging use case in infectious disease patients, detecting Tb based on full blood
441 transcriptomes. Also in this case, SL outperformed individual nodes. Using Tb to simulate
442 scenarios that could be envisioned for building blood transcriptome classifiers for patients
443 during an outbreak situation, we further illustrate the power of SL over individual nodes.
444 Considering the difficulty to quickly negotiate data sharing protocols or contracts during an
445 epidemic or pandemic outbreak, we deduce from these findings that SL would be an ideal
446 strategy for independent producer of medical data to quickly team up to increase the power to
447 generate robust and reliable machine learning-based disease or outcome prediction classifier
448 without the need to share data or relocate data to central cloud storages.

449 In addition, we tested whether we could build a disease prediction classifier for COVID-19 in
450 an outbreak scenario. Building on our knowledge that blood transcriptomes of COVID-19
451 patients are significantly altered with hundreds of genes being changed in expression and with
452 a rather specific signature compared to other infectious diseases[54], we hypothesized that it
453 should be possible to build such a classifier with a rather small number of samples. Here, we
454 provide evidence that classifiers with high accuracy, sensitivity, specificity, and also high F1-
455 statistics can be generated to identify patients with COVID-19 based on their blood
456 transcriptomes. Moreover, we illustrate the power of SL that would allow to quickly increase
457 the power of classifier generation even under very early outbreak scenarios with very few
458 cases used at the training nodes, which could be e.g. collaborating hospitals in an outbreak
459 region. Since data do not have to be shared, additional hospitals could benefit from such a
460 system by applying the classifiers to their new patients and once classified, one could even
461 envision an onboarding of these hospitals for an adaptive classifier improvement schema.
462 Albeit technically feasible, we are fully aware that such scenarios require further classifier
463 testing and confirmation, but also an assessment of how this could be integrated in existing
464 legal and ethical regulations at different regions in the world[5,6]. Furthermore, we appreciate
465 that other currently less expensive data might be suitable for generating classifiers to identify
466 COVID-19 patients[10]. For example, if highly standardized clinical data would become
467 available, SL could be used to interrogate the clinical feature space at many clinics worldwide
468 without any need to exchange the data to develop high performance classifiers for detecting
469 COVID-19 patients. Similarly, recently introduced AI-systems using imaging data[21,22] might be
470 more easily scaled if many hospitals with such data could be connected via SL. Irrespective

471 of these additional opportunities using other parameter spaces, we would like to suggest blood
472 transcriptomics as a promising new alternative due to its very strong signal in COVID-19. A
473 next step will be to determine whether blood transcriptomes taken at early time points could
474 be used to predict severe disease courses, which might allow physicians to introduce novel
475 treatments at an earlier time point. Furthermore, we propose to develop an international
476 database of blood transcriptomes that could be utilized for the development of predictive
477 classifiers in other infectious and non-infectious diseases as well. It could be envisioned that
478 such an SL-based learning scheme could be deployed as a permanent monitoring or early
479 warning system that runs by default, looking for unusual movements in molecular profiles.
480 Collectively, SL together with transcriptomics but also other medical data is a very promising
481 approach to democratize the use of AI among the many stakeholders in the domain of
482 medicine while at the same time resulting in more data privacy, data protection and less data
483 traffic.

484 With increasing efforts to enforce data privacy and security of medical data[8] (hhs.gov,
485 https://www.hhs.gov/hipaa/index.html, 2020; Intersoft Consulting, General Data Protection
486 Regulation, https://gdpr-info.eu) and to reduce data traffic and duplication of large medical
487 data, a decentralized data model will become the preferred choice of handling, storing,
488 managing and analyzing medical data[26]. This will not be restricted to omics data as exemplified
489 here, but will extend to other large medical data such as medical imaging data[55,56]. Particularly
490 in oncology, great successes applying machine learning have already been reported for tumor
491 detection[47,55,57,58], subtyping[59,60], grading[61], genomic characterization[62], or outcome
492 prediction[63], yet progress is hindered by too small datasets at any given institution[26] with
493 current privacy regulations[8] (hhs.gov, https://www.hhs.gov/hipaa/index.html, 2020; Intersoft
494 Consulting, General Data Protection Regulation, https://gdpr-info.ee) making it less appealing
495 to develop centralized AI systems. We introduce Swarm Learning as a decentralized learning
496 system with access to data stored locally that can replace the current paradigm of data sharing
497 and centralized storage while preserving data privacy in cross-institutional research in a wide
498 spectrum of biomedical disciplines. Furthermore, SL can easily inherit developments to further
499 preserve privacy such as functional encryption[64], or encrypted transfer learning approaches[65].
500 In addition, the blockchain technology applied here provides robust measures against semi-
501 honest or dishonest participants/adversaries who might attempt to undermine a Swarm
502 Network. Another important aspect for wide employment of SL in the research community and
503 in real-world applications is the ease of use of the Swarm API, which will make it easier for
504 researchers and developers to include novel developments such as for example private
505 machine learning in TensorFlow[66].

There is no doubt that numerous medical and other data types as well as a vast variety of computational approaches can be used during a pandemic[14]. We do not want to imply that blood transcriptomics would be the preferred solution for the many questions that AI and machine learning could help to solve during such a crisis. Although, at the same time, we have recently shown that blood transcriptomics can be used to define molecular phenotypes of COVID-19, uncover the deviated immune response in severe COVID-19 patients, define unique patterns of the disease in comparison to other diseases and can be utilized to predict potential drugs to be repurposed for COVID-19 therapy (Aschenbrenner et al. unpublished results). Therefore, we explored blood transcriptomics as a unique and rich feature space and a good example to illustrate the advantages of SL in identifying COVID-19 patients. Once larger datasets become available, SL could be used to identify patients at risk to develop severe COVID-19 early after onset of symptoms.

Another important quest that has been proposed is global collaboration and data-sharing[13]. While we could not agree more about the need for global collaboration - an inherent characteristic of SL - we favor systems that do not require data sharing but rather support global collaboration with complete data privacy preservation. Particularly, if using medical data that can also be used to interrogate medical issues unrelated to COVID-19. Indeed, statements by lawmakers have been triggered, clearly indicating that privacy rules also fully apply during the pandemics (EU Digital Solidarity: a call for a pan-European approach against the pandemic, Wojciech Wiewiórowski, https://edps.europa.eu/sites/edp/files/publication/2020-04-06_eu_digital_solidarity_covid19_en.pdf, 2020). Particular in a crisis situation such as the current pandemic, AI systems need to comply with ethical principles and respect human rights[14]. We therefore argue that systems such as Swarm Learning that allow fair, transparent and still highly regulated shared data analytics while preserving data privacy regulations are to be favored, particularly during times of high urgency to develop supportive tools for medical decision making. We therefore also propose to explore SL for image-based diagnostics of COVID-19 from patterns in X-ray images or computed tomography (CT) scans[21,22], structured health records[67], or wearables for disease tracking[14]. Swarm learning would also have the advantage that model and code sharing as well as dissemination of new applications is easily scalable, because onboarding of new swarm participants is structured by blockchain technology, while scaling of data sharing is not even necessary due the inherent local computing of the data[14]. Furthermore, swarm learning can reduce the burden of establishing global, comprehensive, open, and verified datasets.

Collectively, we introduce Swarm Learning defined by the combination of blockchain technology and decentralized machine learning in an entirely democratized approach

eliminating a central player and therefore representing a uniquely fitting strategy for the inherently locally organized domain of medicine. We used blood transcriptomes in three scenarios as use cases since they combine blood as the most widely used surrogate tissue for diagnostic purposes with an omics technology producing high-dimensional data with many parameters. Since the deployment of Swarm Learning due to ease of use of Swarm Learning libraries is a rather simple task, we propose to expand the use of this technology and further develop such classifiers in a unifying fashion across centers worldwide without any need to share the data itself. Our use cases are supposed to serve as examples for other high-dimensional data in the domain of medicine, but certainly also many other areas of research and application against the pandemics and beyond.

Acknowledgments:

We thank Dr. Sach Mukherjee (Statistics and Machine Learning, German Center for Neurodegenerative Diseases) for feedback on the manuscript.

Deutsche COVID-19 Omics Initiative (DeCOI)

Robert Bals, Alexander Bartholomäus, Anke Becker, Ezio Bonifacio, Peer Bork, Thomas Clavel, Maria Colome-Tatche, Andreas Diefenbach, Alexander Dilthey, Nicole Fischer, Konrad Förstner, Julien Gagneur, Alexander Goesmann, Torsten Hain, Michael Hummel, Stefan Janssen, René Kallies, Birte Kehr, Andreas Keller, Sarah Kim-Hellmuth, Christoph Klein, Oliver Kohlbacher, Jan Korbel, Ingo Kurth, Markus Landthaler, Yang Li, Kerstin Ludwig, Oliwia Makarewicz, Manja Marz, Alice McHardy, Christian Mertes, Markus Nöthen, Peter Nürnberg, Uwe Ohler, Stephan Ossowski, Jörg Overmann, Klaus Pfeffer, Alfred Pühler, Nikolaus Rajewsky, Markus Ralser, Olaf Rieß, Stephan Ripke, Ulisses Nunes da Rocha, Philip Rosenstiel, Antoine-Emmanuel Saliba, Leif Erik Sander, Birgit Sawitzki, Philipp Schiffer, Joachim L. Schultze, Alexander Sczyrba, Oliver Stegle, Jens Stoye, Fabian Theis, Janne Vehreschild, Jörg Vogel, Max von Kleist, Andreas Walker, Jörn Walter, Dagmar Wieczorek, John Ziebuhr

Funding:

This work was supported in part by the German Research Foundation (DFG) to J.L.S. (INST 37/1049-1, INST 216/981-1, INST 257/605-1, INST 269/768-1 and INST 217/988-1, INST 217/577-1); the HGF grant sparse2big, the EU projects SYSCID (grant number 733100) and ImmunoSep, and by HPE to the DZNE for generating whole blood transcriptome data from patients with COVID-19. Sofia Ktena is supported by the Hellenic Institute for the Study of Sepsis. The clinical study in Greece was supported by the Hellenic Institute for the Study of Sepsis. E.J.G.-B. received funding from the FrameWork 7 program HemoSpec (granted to the National and Kapodistrian University of Athens), the Horizon2020 Marie-Curie Project European Sepsis Academy (granted to the National and Kapodistrian University of Athens), and the Horizon 2020 European Grant ImmunoSep (granted to the Hellenic Institute for the Study of Sepsis).

Author contributions:

Conceptualization, J.L.S; K.L.S, S.Ma.; Methodology, S.W.-H., C.S., R.S., M.D., B.M., C.M.S.; Software: M.L.; V.G, C.S., S.Ma., S.Mu.; Investigation, S.W.-H., K.S., M.K., A.D., M.N., H.T., T.U.; Biospecimen/ enzyme resources, M.K., P.P., M.G.N., S.K., E.G.-B., M.M.B.BM., C.K., M.G.; Writing – Original Draft, S.W.-H., H.S., K.L.S., M.B., J.L.S.; Writing – Review & Editing, S.W.-H., H.S., K.L.S., D.S., A.C.A., M.K., P.P., M.G.N., M.B., S.C., M.S.W., E.L.G., J.L.S.; Visualization, H.S., J.L.S; Supervision, H.S., K.L.S., J.L.S.; Project Administration, H.S., J.L.S.; Funding Acquisition, W.F., J.L.S., F.J.T., J.H., N.Y., A.K.S., M.G., and M.M.B.B.

Ethics declarations

Competing Interests

H.S., K.L.S, S.Ma., S.Mu., V.G., R.S., C.S., M.D., B.M, C.M.S., S.C., M.S.W, E.L.G are employees of Hewlett Packard Enterprise. Hewlett Packard Enterprise developed the Swarm Learning Library in its entirety as described in this work and has submitted multiple associated patent applications. E.J.G.-B. received honoraria from AbbVie USA, Abbott CH, InflaRx GmbH, MSD Greece, XBiotech Inc. and Angelini Italy; independent educational grants from AbbVie, Abbott, Astellas Pharma Europe, AxisShield, bioMérieux Inc, InflaRx GmbH, and XBiotech Inc.

Figures and Figure Legends

Figure 1

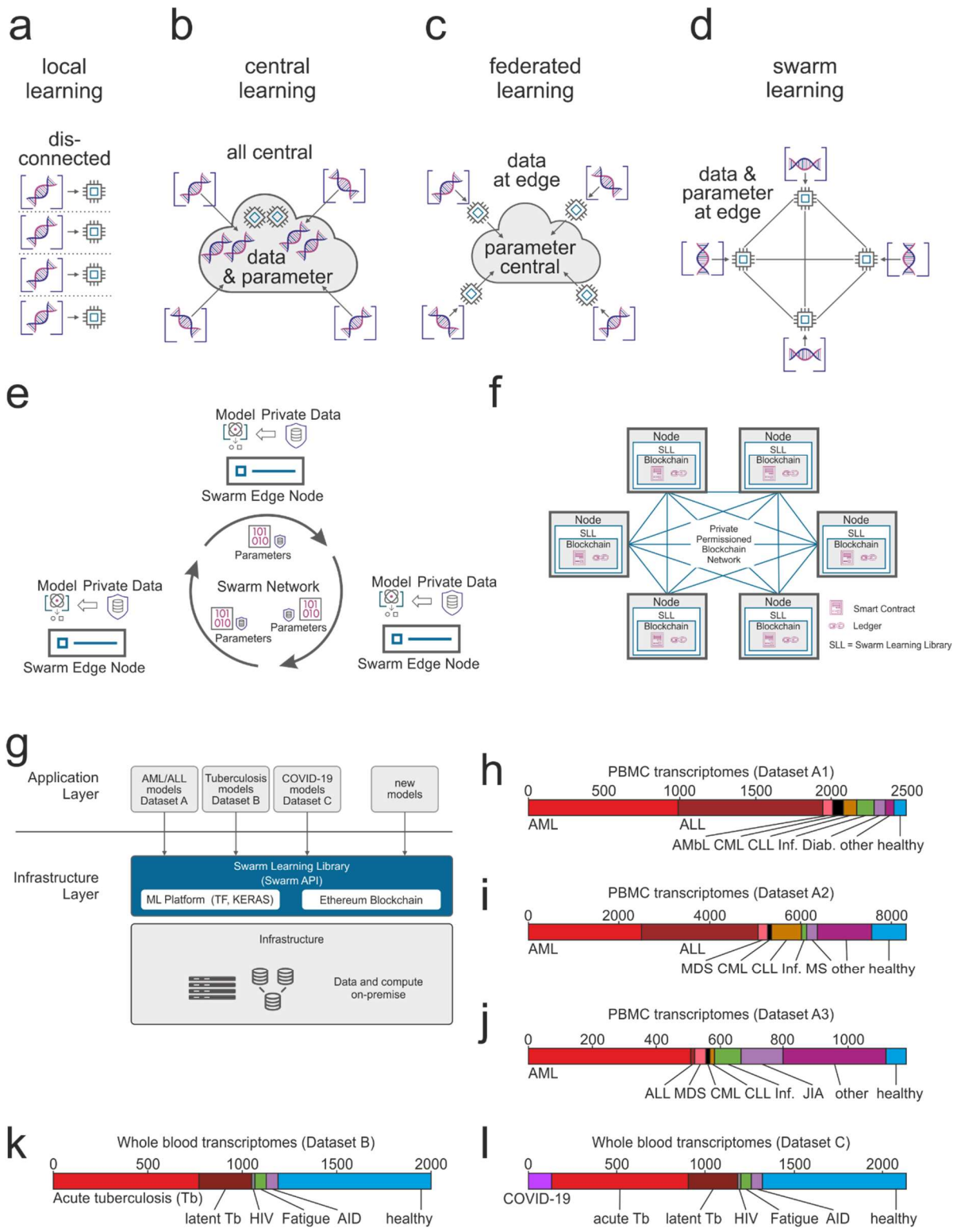

605 **Figure 1. Concept of Swarm Learning**

606 **(a-d)** The principles of Swarm Learning in contrast to other machine learning concepts. **(a)**
607 Illustration of the concept of local learning with data and computation at different, but
608 disconnected locations. **(b)** Principle of cloud-based machine learning where data from
609 contributing centers move copies of the data to a central cloud-based storage; centrally
610 located data are then used for central - often cloud-based - machine learning. **(c)** Federated
611 learning with data being kept with the data contributor and computing is also performed at the
612 site of local data storage and availability, yet parameter settings of machine learning are
613 orchestrated by a central parameter server. **(d)** Swarm Learning principle with swarm nodes
614 being connected in a democratic fashion (enabled by blockchain technology) without the need
615 for a central custodian or parameter server. Data privacy is preserved, data is kept where it is
616 generated, computation is achieved locally and learning parameters are shared within the
617 Swarm Network. **(e)** Schematic representation of the Swarm Network consisting of the Swarm
618 Edge Nodes (short 'nodes') that exchange parameters for learning, which is implemented
619 using blockchain technology. Use of private data at each node together with the model
620 provided via Swarm Network. **(f)** Concept and outline of the private permissioned blockchain
621 network as a layer of the Swarm Learning network. Each node consists of the blockchain,
622 including the ledger and smart contract, as well as the Swarm Learning Library (SLL) with the
623 API to interact with other nodes within the network. **(g)** Application and infrastructure layer as
624 part of the Swarm Learning concept. **(h-l)** Description of the transcriptome datasets used
625 within this study: Dataset **(h)** A1 and **(i)** A2, two microarray-based transcriptome datasets of
626 peripheral blood mononuclear cells (PBMC). **(j)** Dataset A3, RNA-seq based transcriptomes
627 of PBMC. Dataset **(k)** B and **(l)** C, RNA-seq based whole blood transcriptome datasets.
628 Abbreviations: *AML*, Acute Myeloid Leukemia; *ALL*, Acute Lymphoblastic Leukemia; *COVID-*
629 *19*, CoronaVirus Disease 2019; *API*, Application Programming Interface; ML, Machine
630 Learning; TF, Tensor Flow; KERAS, Open Source Deep Learning Library; *AMbl*, Acute
631 Myeloblastic Leukemia; *CML*, Chronic Myeloid Leukemia; *CLL*, Chronic Lymphocytic
632 Leukemia; *Inf*., Infections, *Diab*., Diabetes Type II; *MDS*, Myelodysplastic Syndrome; *MS*,
633 multiple sclerosis; *JIA*, Juvenile idiopathic arthritis; *Tb*, tuberculosis; *HIV*, Human
634 Immunodeficiency Virus, *AID*, Acute Infectious Disease. SLL Swarm Learning Library.

Figure 2

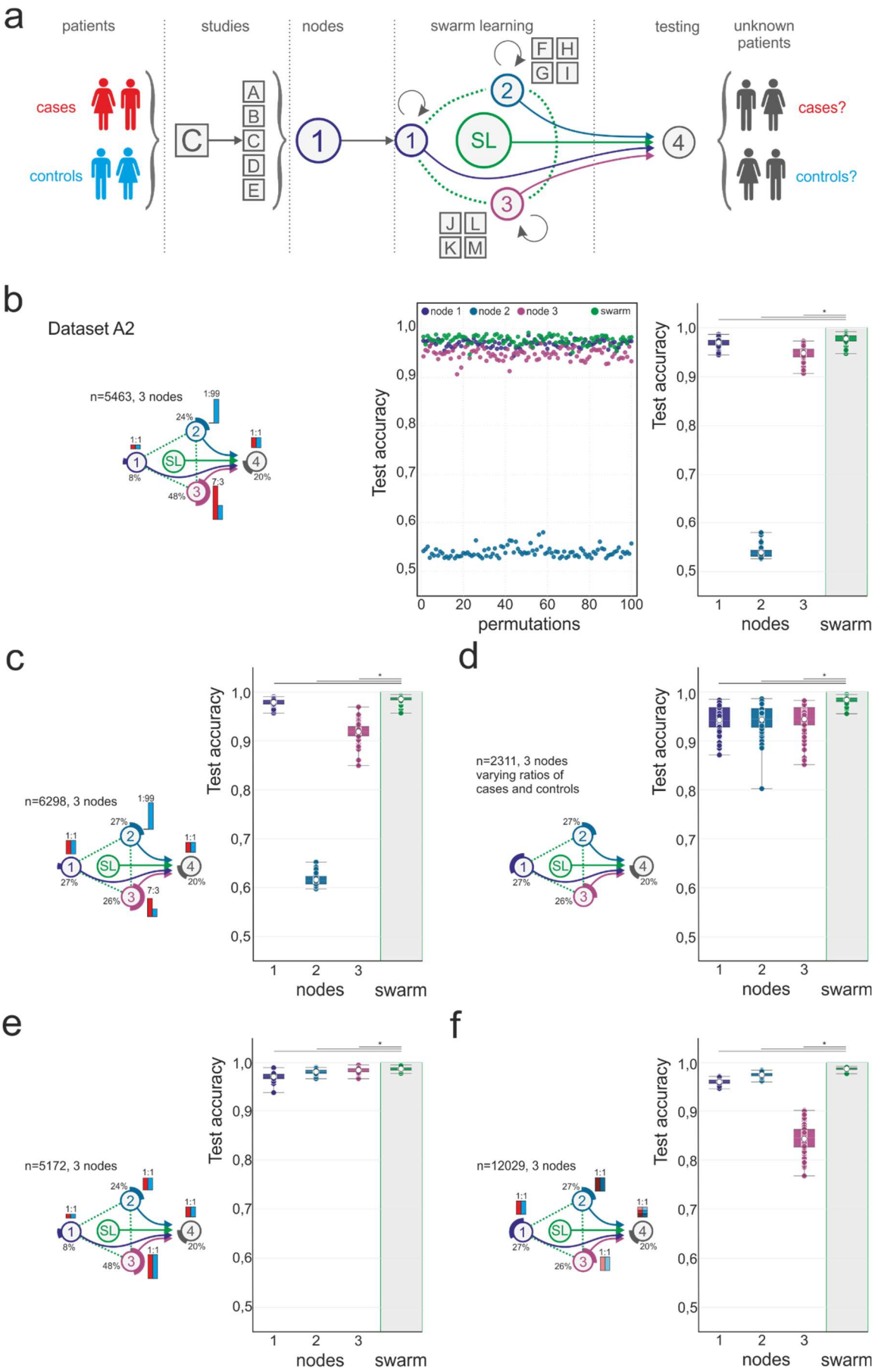
a
patients
studies
nodes
swarm learning
testing
unknown patients
cases
controls
C
A
B
C
D
E
1
2
3
4
SL
F
H
G
I
J
L
K
M
cases?
controls?
b
Dataset A2
n=5463, 3 nodes
node 1
node 2
node 3
swarm
Test accuracy
permutations
nodes
swarm
c
n=6298, 3 nodes
d
n=2311, 3 nodes
varying ratios of
cases and controls
e
n=5172, 3 nodes
f
n=12029, 3 nodes

635

636 **Figure 2. Swarm learning to predict leukemias from PBMC data**

637 **(a)** Schematic representation of the use of the transcriptome data derived from more than
638 12,000 individuals in over 100 individual studies[47]. Principle of distribution of data to individual
639 Swarm Edge Nodes (short 'nodes'). Nodes 1-3 were used for training, node 4 for testing.
640 Swarm Learning (SL) was achieved by integrating nodes 1-3 for training following procedures
641 described in detail in Supplementary Information. **(b)** Scenario using Dataset A2. Left panel
642 illustrating the setting of the scenario concerning distribution of cases and controls to individual
643 nodes, as well as total number of samples used for this scenario. Cases (red bar) and controls
644 (blue bar) were distributed unevenly among nodes, the number of samples distributed to each
645 node was also uneven in this scenario. Middle panel shows results of accuracy of all 100
646 permutations performed for the 3 training nodes individually as well as the results obtained by
647 SL. Accuracy is defined for the independent fourth node used for testing only. Right panel
648 represents box-whisker plot representation of the individual data presented in the middle panel
649 showing mean, 1st and 3rd quartile and whisker type Min/Max. **(c)** Scenario with uneven
650 numbers of cases and controls at the different training nodes but similar numbers of samples
651 at each node to determine impact of these changes on SL performance. Left panel: schematic
652 representation of scenario and right panel: results obtained for accuracy at the test node (node
653 4) for each of the three training nodes 1-3 and SL independently as box and whisker plot with
654 the same parameter as described for (b). **(d)** Scenario with even numbers at each of the
655 nodes, schematic representation (left panel) and visualization of results as box-whisker plots
656 as in (b) and (c). **(e)** Scenario with even distribution of cases and controls at each training
657 node, but different numbers of samples at each node and overall increase in numbers of
658 samples. Representation of schema and data visualization as in (b-d). **(f)** Scenario where each
659 node obtained samples from different Datasets (node 1: Dataset A1, node 2: Dataset A2, node
660 3, Dataset A3). Node 4 obtained samples from each Dataset A1-A3 to define impact on
661 technical bias on Swarm Learning performance. Representation of schema and data
662 visualization as in (b-e). Statistical differences between results derived by SL and individual
663 nodes including all permutations performed were calculated with Wilcoxon signed rank test
664 with continuity correction; asterisk and line: $p<0.05$.

Figure 3

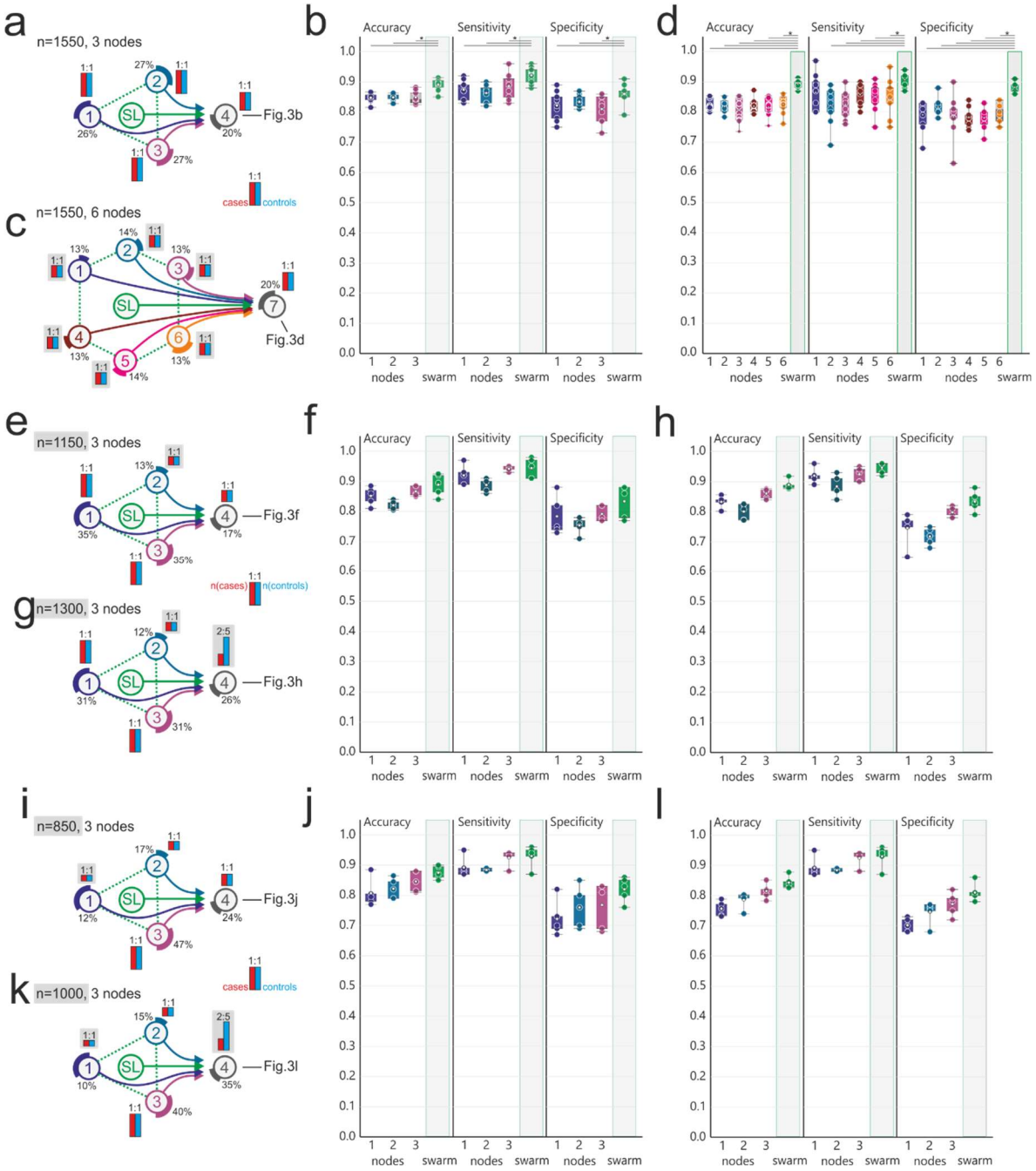
a
n=1550, 3 nodes
Fig.3b
cases
controls
c
n=1550, 6 nodes
Fig.3d
b
d
Accuracy
Sensitivity
Specificity
nodes
swarm
e
n=1150, 3 nodes
Fig.3f
n(cases)
n(controls)
g
n=1300, 3 nodes
Fig.3h
f
h
i
n=850, 3 nodes
Fig.3j
k
n=1000, 3 nodes
Fig.3l
j
l

Figure 3. Swarm learning to identify patients with tuberculosis

(a-l) Principle of distribution of data to individual Swarm Edge Nodes (short 'nodes'). Nodes 1-3 were used for training, node 4 for testing. Swarm Learning (SL) was achieved by integrating nodes 1-3 for training following procedures described in detail in Supplementary Information. All scenarios use dataset B and use acute TB as case and the remaining samples as controls. Left panels **(a,c,e,g,i,k)** illustrate the setting of the scenarios concerning distribution of cases (red bar) and controls (blue bar) to individual nodes, as well as total number of samples used for the scenario. Percentage at each node reflects the use of samples out of the complete dataset. **(a)** Scenario with even number of cases at each training node and the test node. **(b)** Evaluation of the scenario presented in (a) showing accuracy, sensitivity and specificity of five permutations for each training node and SL at node 4 (test node) as box-whisker plot (mean, 1st and 3rd quartile, whisker type Min/Max). **(c)** Scenario similar to (a) but with six training nodes. **(d)** Evaluation of scenario (c) as described in (b) but for all six training nodes. **(e)** Scenario where the training nodes have evenly distributed numbers of cases and controls at each training node, but node 2 has lower numbers of samples. **(f)** Evaluation of scenario (e) as described in (b). **(g)** Scenario similar to (e) but with reduced prevalence at the test node. **(h)** Evaluation of scenario (g) as described in (b). **(i)** Scenario with even distribution of cases and controls at each training node, but node 1 only has a very small training set. The test set is evenly distributed. **(j)** Evaluation of scenario (i) as described in (b). **(k)** Scenario similar to (i) but with uneven distribution in the test node. **(l)** Evaluation of scenario (k) as described in (b). Statistical differences between results derived by SL and individual nodes including all permutations performed were calculated with Wilcoxon signed rank test with continuity correction; asterisk and line: $p<0.05$.

Figure 4

a

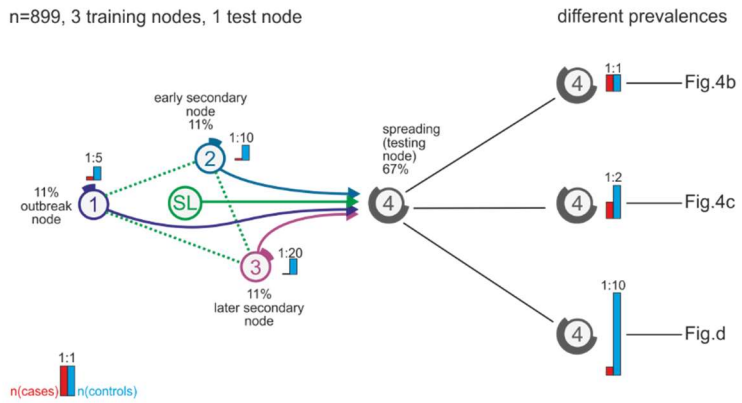

b

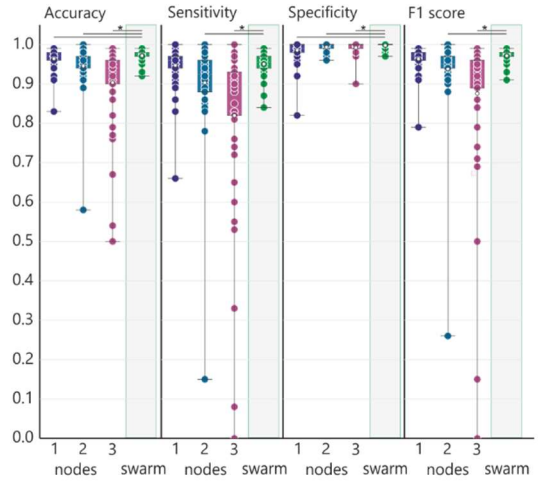

c

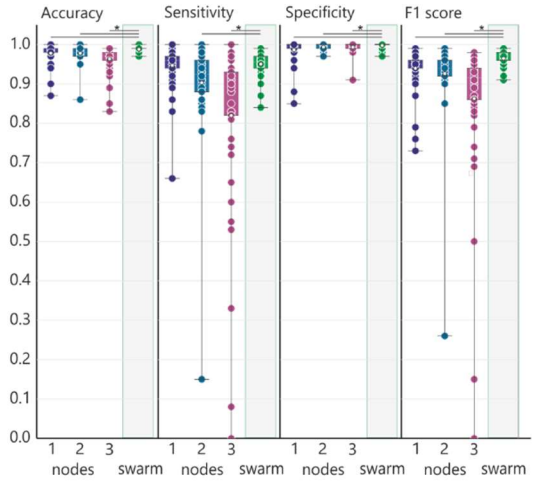

d

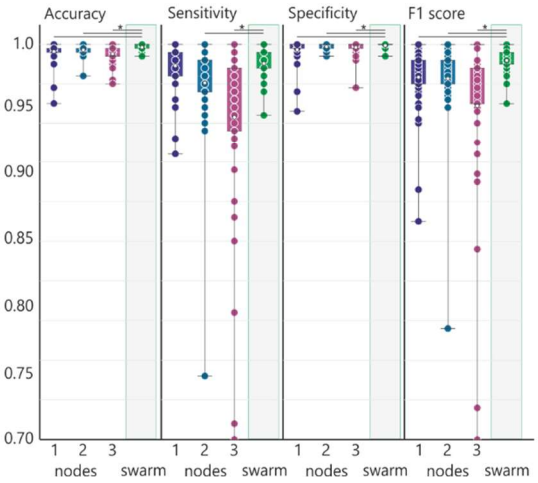

692 **Figure 4. Identification of COVID-19 patients in an outbreak scenario**

693 **(a)** Description of an outbreak scenario for COVID-19 using Dataset C. Nodes 1-3 were used
694 for training, node 4 for testing. Swarm Learning (SL) was achieved by integrating nodes 1-3
695 for training following procedures described in detail in Supplementary Information. COVID-19
696 samples were used as cases. In this scenario, node 1 would be the outbreak node with the
697 highest prevalence. Training node 2 has fewer cases and is an early secondary node, and
698 node 3 acts as a later secondary node. The spreading is tested on the testing node with three
699 different prevalences (**b,c,d**) and shown as box-whisker plot (mean, 1st and 3rd quartile,
700 whisker type Min/Max). **(b)** Evaluation of (a) with even prevalence showing accuracy,
701 sensitivity, specificity and F1-score of fifty permutations for each training node and the SL
702 (node 4). **(c)** Evaluation (as described in (b)) of scenario (a) using a 1:2 ratio for cases and
703 controls in the test set. **(d)** Evaluation (as described in (b)) of scenario (a) using a 1:10 ratio in
704 the test set to simulate detection in regions with new infections. Statistical differences between
705 results derived by SL and individual nodes including all permutations performed were
706 calculated with Wilcoxon signed rank test with continuity correction; asterisk and line: $p<0.05$.

Extended Data Figure 1

a

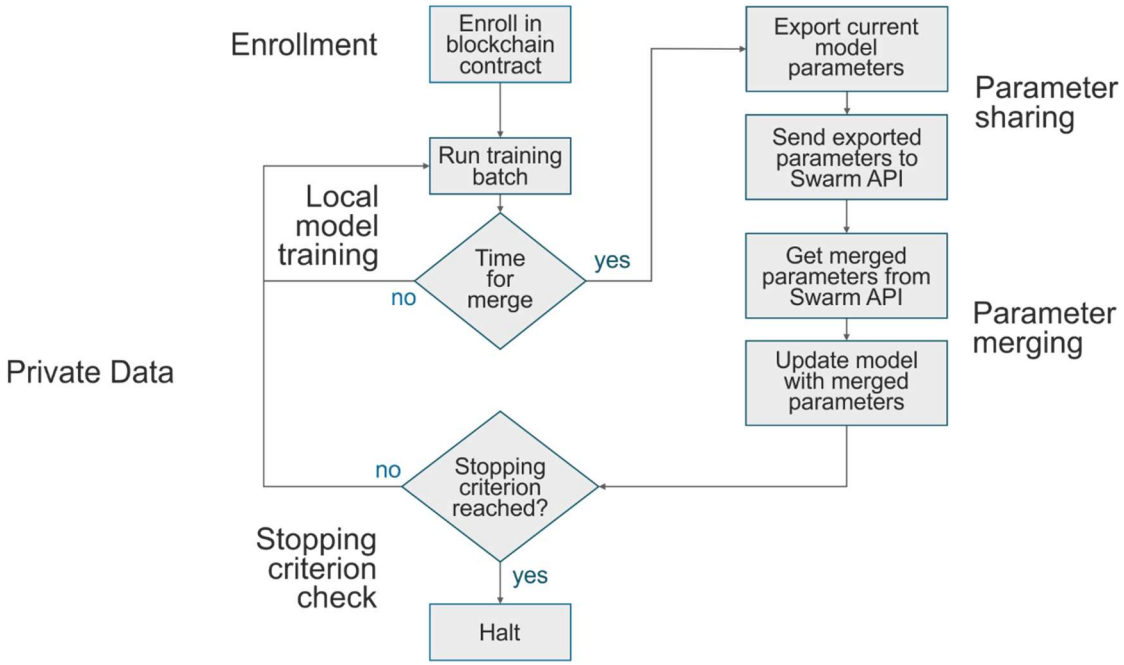

Extended Data Figure 1. corresponding to Fig. 1

Schematics of the principles of the workflow of Swarm Learning once the nodes have been enrolled within the Swarm Network via private permissioned blockchain contract.

Extended Data Figure 2

a

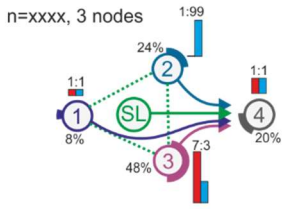

b

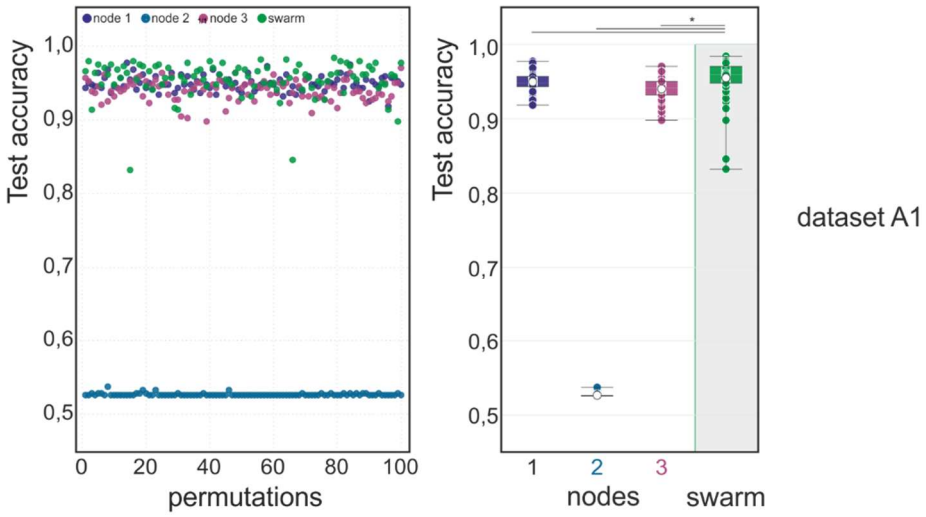

dataset A1

c

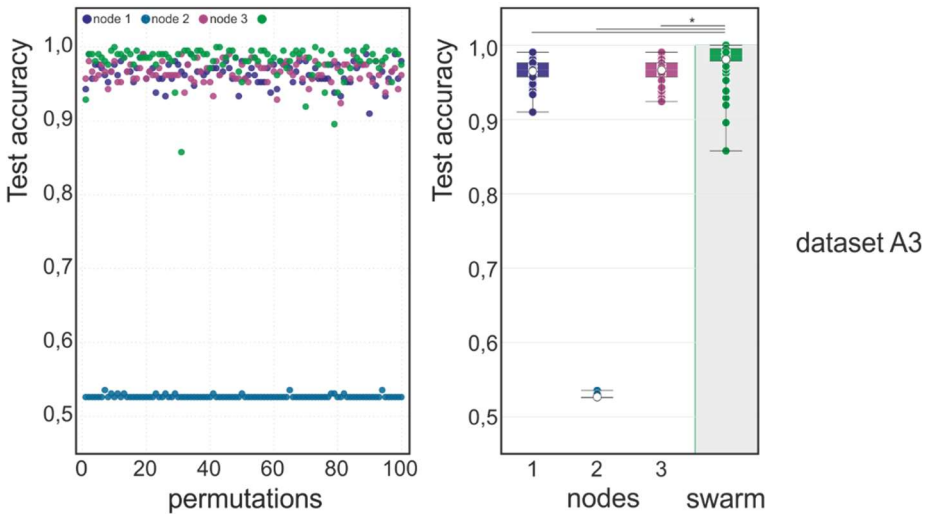

dataset A3

715 **Extended Data Figure 2. Scenario corresponding to Fig. 2b in dataset A1 and A3**

716 Main settings are identical to what is described in Fig. 2 for Dataset A2. **(a)** Scenario with
717 different prevalence of AML and different number of samples at each training node. The test
718 set has an even distribution. **(b)** Evaluation of test accuracy for 100 permutations of dataset
719 A1 per node and swarm. **(c)** Evaluation using dataset A3. Statistical differences between
720 results derived by SL and individual nodes including all permutations performed were
721 calculated with Wilcoxon signed rank test with continuity correction; asterisk and line: $p<0.05$.

Extended Data Figure 3

a

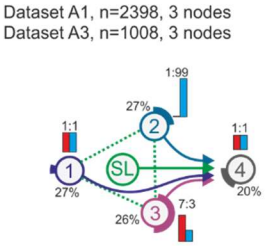

b

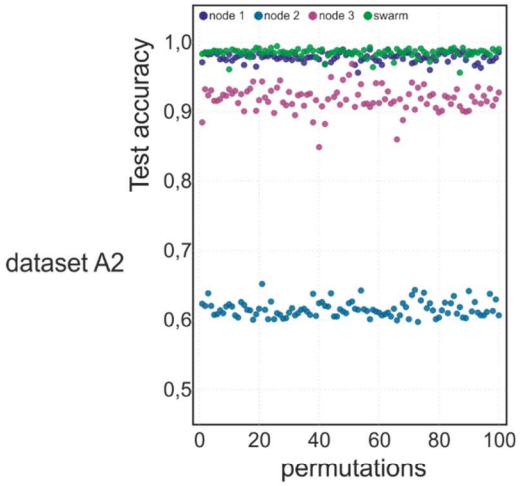

c

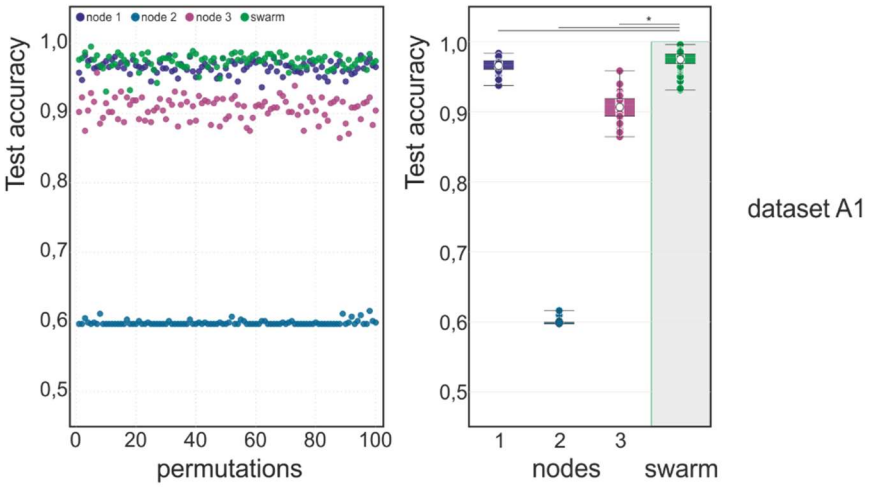

d

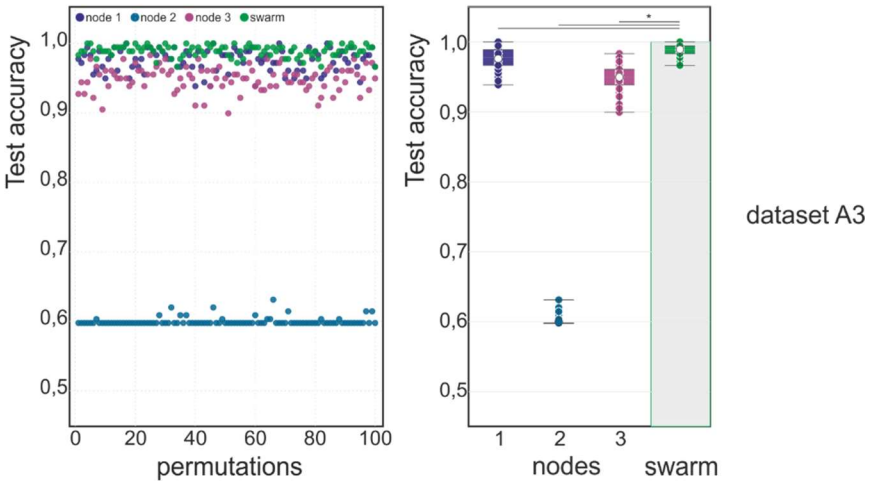

723 **Extended Data Figure 3. Scenario corresponding to Fig. 2c in dataset A1 and A3**

724 Main settings are identical to what is described in Fig. 2 for dataset A2. **(a)** Scenario with
725 similar training set sizes per node but decreasing prevalence. The test set ratio is 1:1. **(b)**
726 Evaluation of the test accuracy over 100 permutation for dataset A2 (corresponding to Fig.
727 2c). **(c)** Evaluation of the test accuracy over 100 permutation for dataset A1. **(d)** Evaluation of
728 the test accuracy over 100 permutation for dataset A3. Box-whisker plots (mean, 1st and 3rd
729 quartile, whisker type Min/Max). Statistical differences between results derived by SL and
730 individual nodes including all permutations performed were calculated with Wilcoxon signed
731 rank test with continuity correction; asterisk and line: $p<0.05$.

Extended Data Figure 4

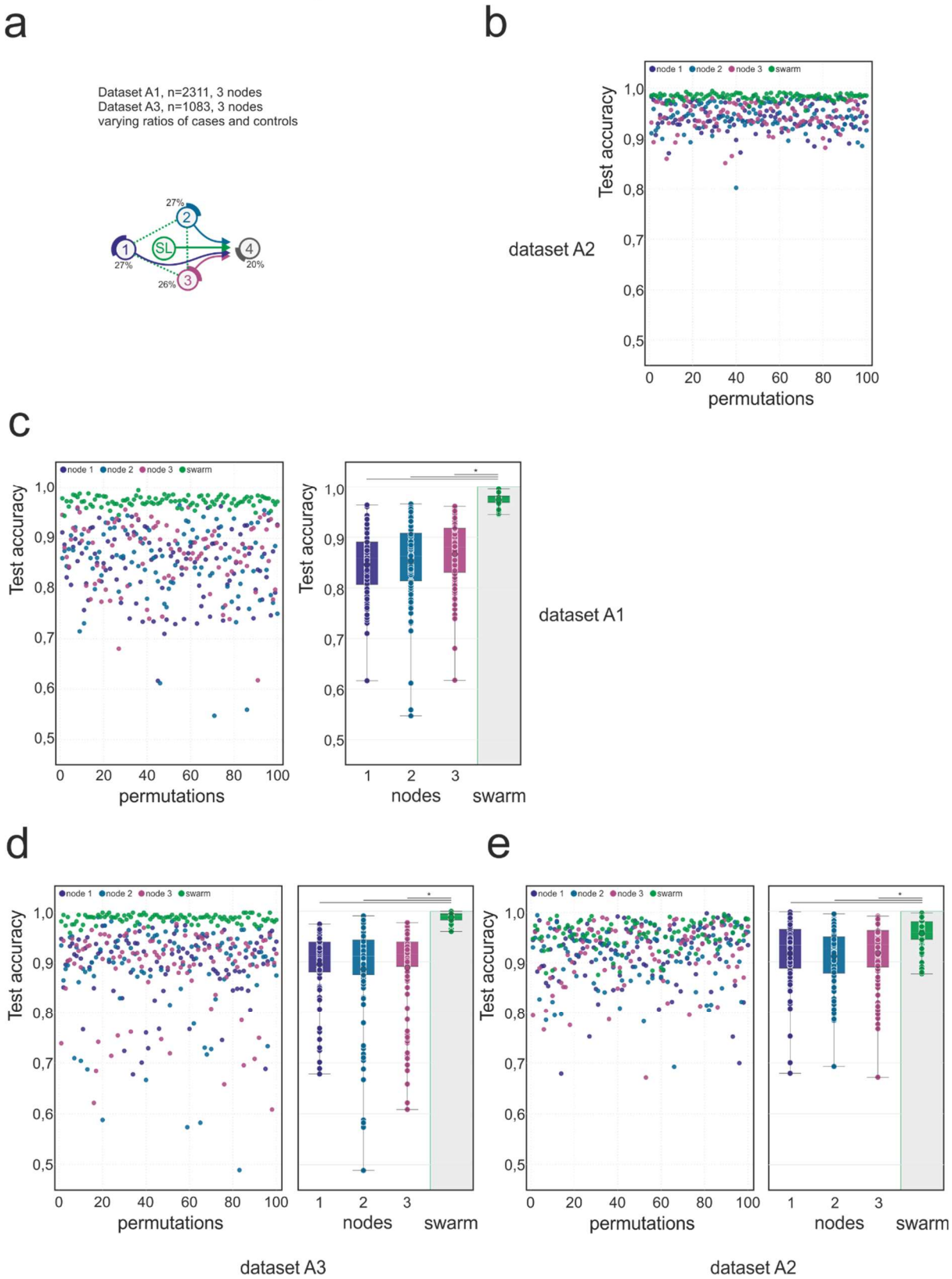

734 **Extended Data Figure 4. Scenario corresponding to Fig. 2d in dataset A1 and A3**

735 Main settings are identical to what is described in Fig. 2 for dataset A2. (a) Scenario with
736 similar sample sizes among three nodes, but with independent studies at each training node.
737 Case and control ratios varied for each permutation. Testing samples are sampled from the
738 studies also present in the training data. **(b)** Evaluation of the test accuracy over 100
739 permutation for dataset A2 (corresponding to Fig. 2d). **(c)** Evaluation of the test accuracy over
740 100 permutation for dataset A1. **(d)** Evaluation of the test accuracy over 100 permutation for
741 dataset A3. **(e)** In this scenario, samples at the test node were derived from published studies
742 completely independent from the studies used for training at the training nodes. Evaluation of
743 the test accuracy over 100 permutation for dataset A2. Box-whisker plots (mean, 1st and 3rd
744 quartile, whisker type Min/Max). Statistical differences between results derived by SL and
745 individual nodes including all permutations performed were calculated with Wilcoxon signed
746 rank test with continuity correction; asterisk and line: $p<0.05$.

Extended Data Figure 5

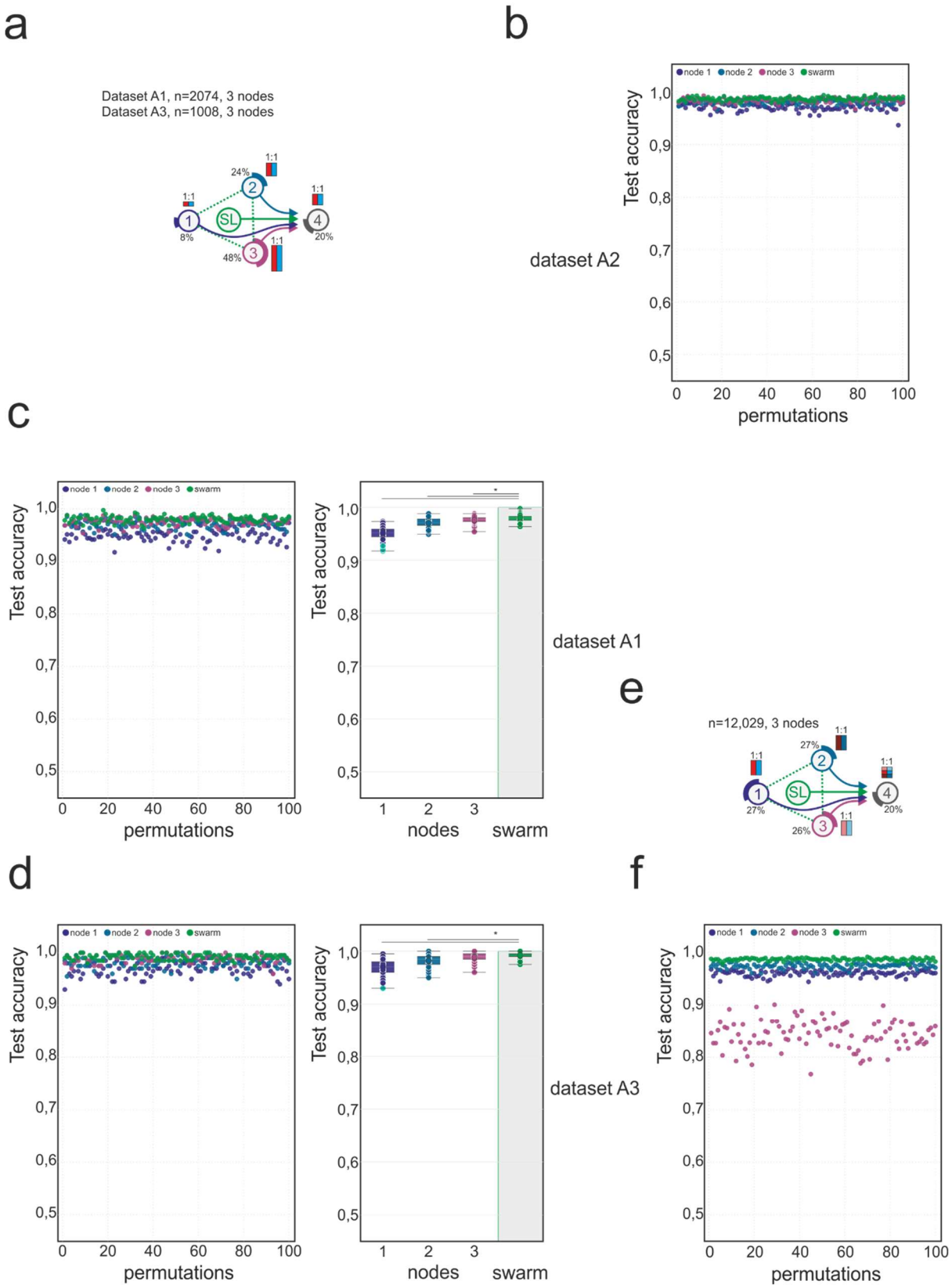

749 **Extended Data Figure 5. Scenario corresponding to Fig. 2e in dataset A1 and A3**

750 Main settings are identical to what is described in Fig. 2 for dataset A2. **(a)** The case:control
751 distribution is even, the training sets increase from node 1 to node 3. The test set is evenly
752 split. **(b)** Test accuracy for evaluation of dataset A2 (corresponding to Fig. 2e). **(c)** Test
753 accuracy for evaluation of dataset A1. **(d)** Test accuracy for evaluation of dataset A3. **(e)**
754 Scenario where the data sets A1, A2, and A3 are assigned to a single training node each.
755 Scenario similar to (a) but with equal training set sizes. **(f)** Evaluation results of 100
756 permutations (corresponding to Fig. 2f). Box-whisker plots (mean, 1st and 3rd quartile, whisker
757 type Min/Max). Statistical differences between results derived by SL and individual nodes
758 including all permutations performed were calculated with Wilcoxon signed rank test with
759 continuity correction; asterisk and line: $p<0.05$.

Extended Data Figure 6

a

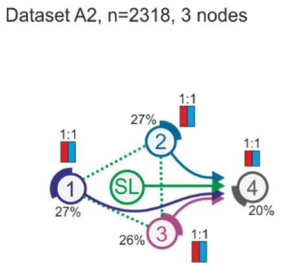

b

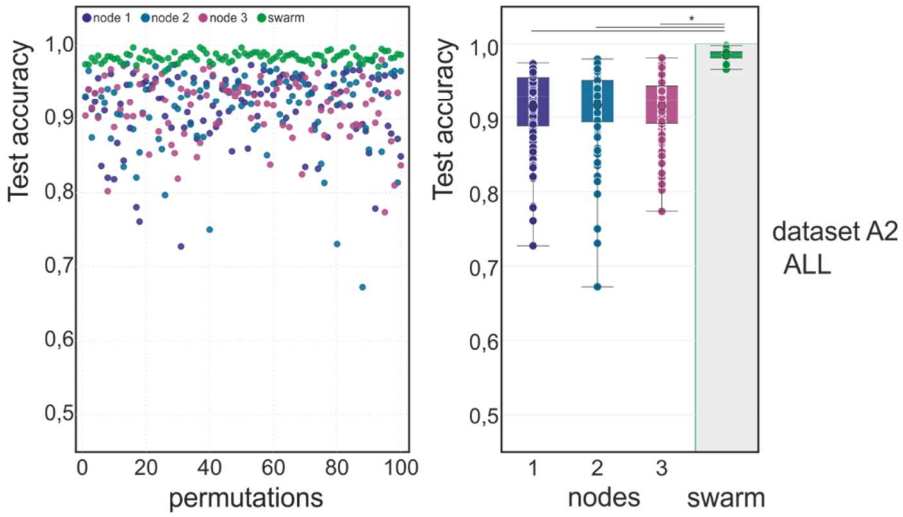

762 **Extended Data Figure 6. Scenario for ALL in dataset 2**

763 Main settings are identical to what is described in Fig. 2 for dataset A2. Here cases are
764 samples derived from patients with ALL, while all other samples are controls (including AML).
765 **(a)** Scenario for the detection of ALL in dataset A2. The training sets are evenly distributed
766 among the nodes. The test ratio is 1:1. **(b)** Evaluation of scenario (a) for test accuracy over
767 100 permutations. Box-whisker plot (mean, 1st and 3rd quartile, whisker type Min/Max).
768 Statistical differences between results derived by SL and individual nodes including all
769 permutations performed were calculated with Wilcoxon signed rank test with continuity
770 correction; asterisk and line: $p<0.05$.

Extended Data Figure 7

a group settings in use case 2 (tuberculosis)

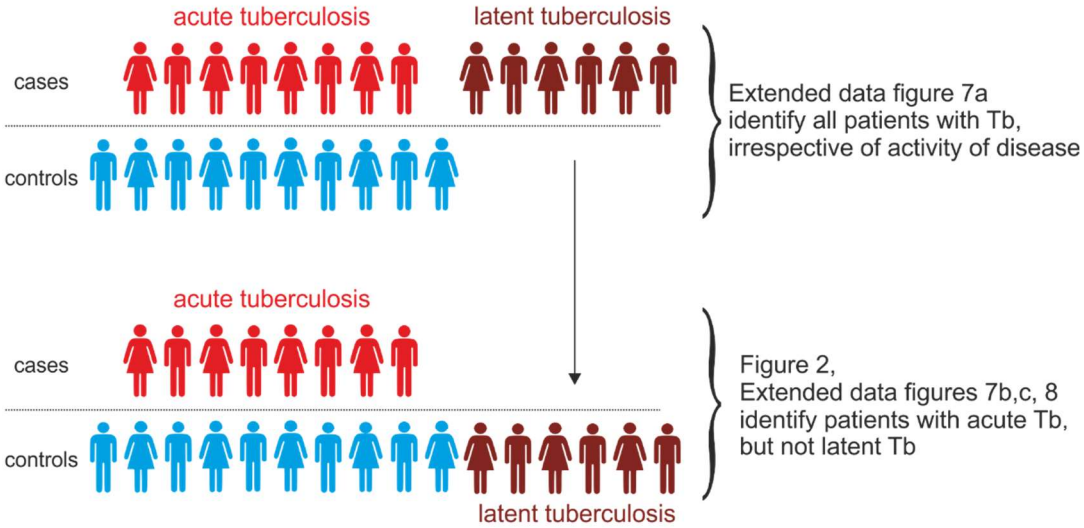

b

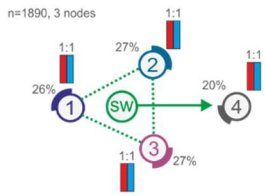

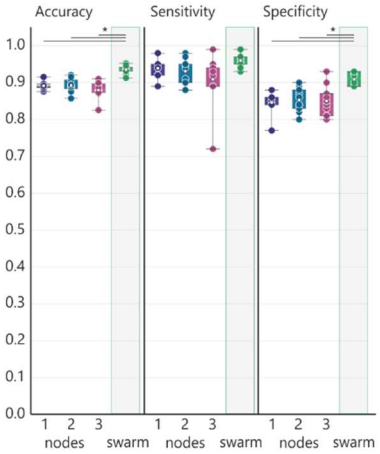

Only scenario for which the following applies:
acute **and** latent TB are cases
versus
controls

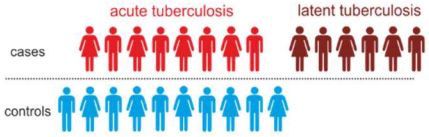

c

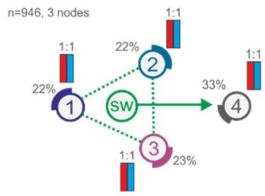

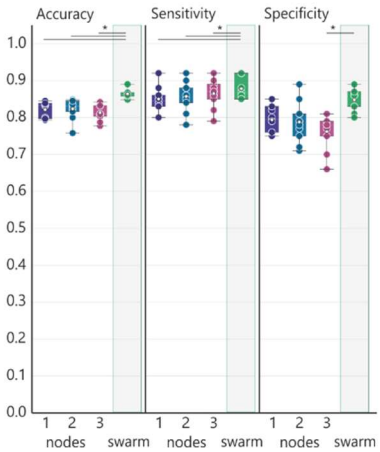

All other scenarios:
Only acute TB cases
versus
controls (now also including latent Tb cases)

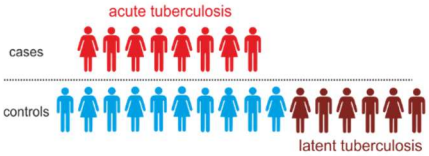

Extended Data Figure 7. Scenario for detecting all Tb versus controls

(a) Description of the different group settings used based on the assignment of latent Tb to control or case. **(b)** Evaluation of a scenario where acute and latent Tb are cases. The data is evenly distributed among the training nodes. The scenario is evaluated as described in Figure 3 (b). **(c)** Scenario designed similar to (b) but latent Tb is part of control. Box-whisker plot (mean, 1st and 3rd quartile, whisker type Min/Max). Statistical differences between results derived by SL and individual nodes including all permutations performed were calculated with Wilcoxon signed rank test with continuity correction; asterisk and line: $p<0.05$.

Extended Data Figure 8

a

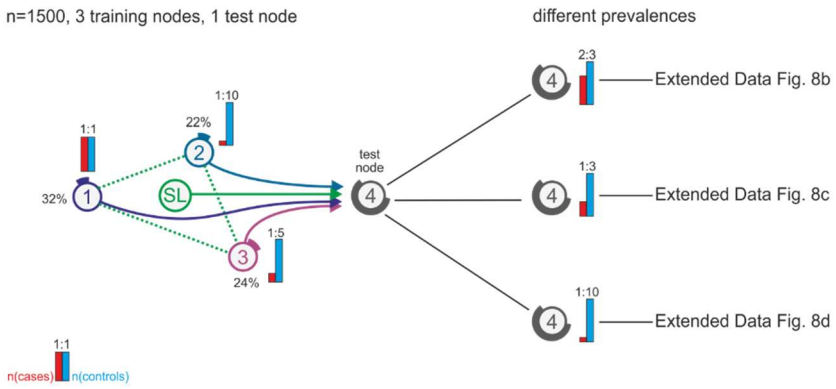

b

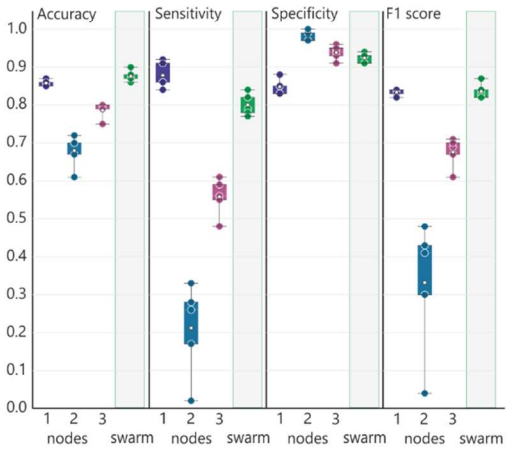

c

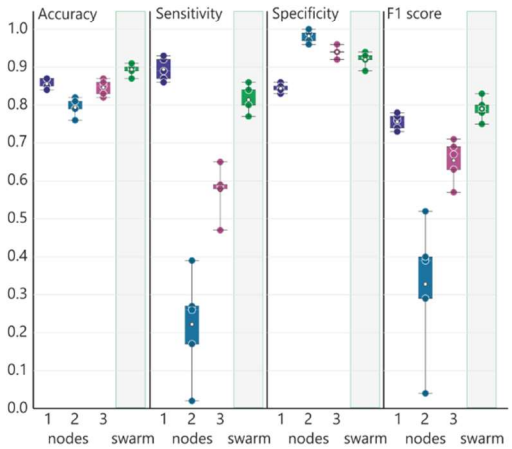

d

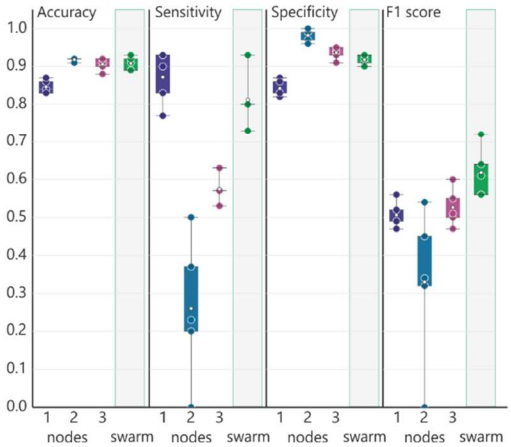

Extended Data Figure 8: Scenario detecting acute Tb with low prevalence at training nodes

(a) Scenario with training nodes having different prevalence: node 2 has only a 1:10 ratio. Three prevalence scenarios are used in the test set. **(b)** Evaluation of scenario (a) showing accuracy, sensitivity, specificity and F1 score. **(c)** Similar scenario as in (a) but prevalence changed to 1:3 cases: controls in the training set. **(d)** Similar scenario as in (a) but prevalence changed to 1:10 cases: controls in the training set. Box-whisker plot (mean, 1st and 3rd quartile, whisker type Min/Max). Statistical differences between results derived by SL and individual nodes including all permutations performed were calculated with Wilcoxon signed rank test with continuity correction; asterisk and line: $p<0.05$.

Extended Data Figure 9

a

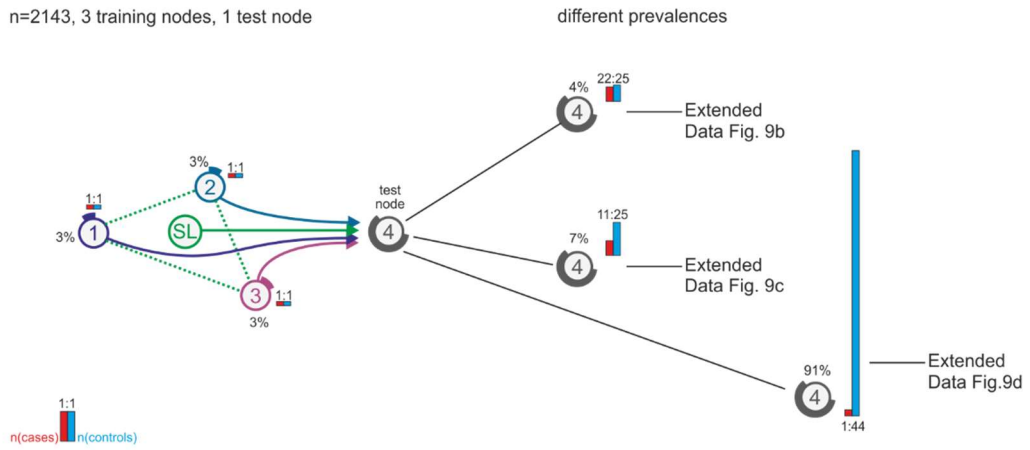

b

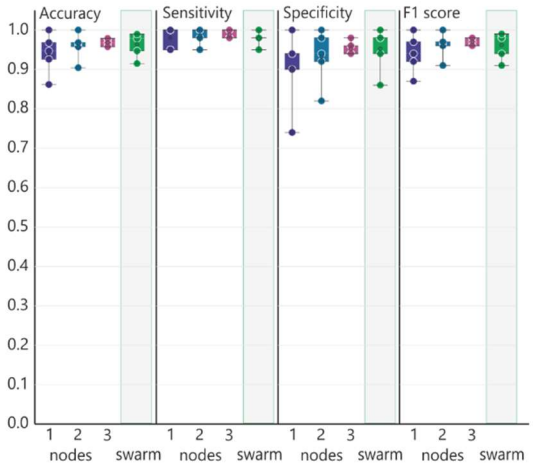

c

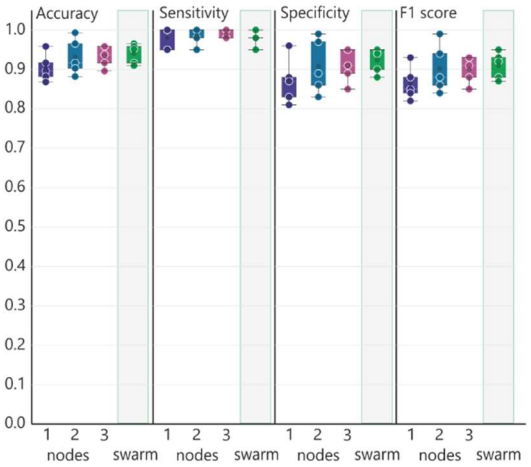

d

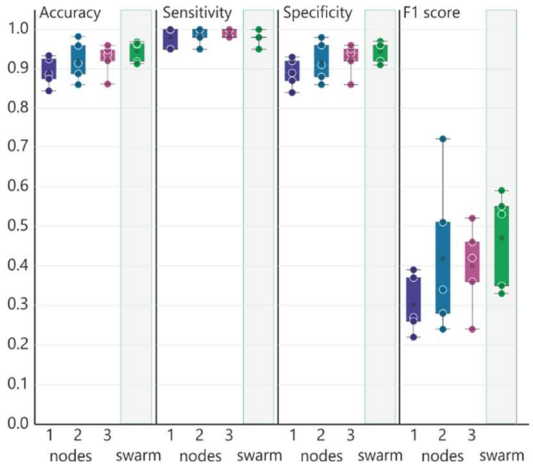

Extended Data Figure 9. Baseline scenario for detecting COVID-19 patients

(a) Scenario with even training set distribution among nodes 1-3. Three different testing sets with different prevalence are simulated. **(b)** Evaluation of (a) for a 22:25 case: control ratio showing accuracy, sensitivity, specificity and F1 score. **(c)** Evaluation results of scenario (a) for a 11:25 ratio. **(d)** Evaluation results of scenario (a) for a 1:44 prevalence. Box-whisker plot (mean, 1st and 3rd quartile, whisker type Min/Max). Statistical differences between results derived by SL and individual nodes including all permutations performed were calculated with Wilcoxon signed rank test with continuity correction; asterisk and line: $p<0.05$.

Extended Data Figure 10

a

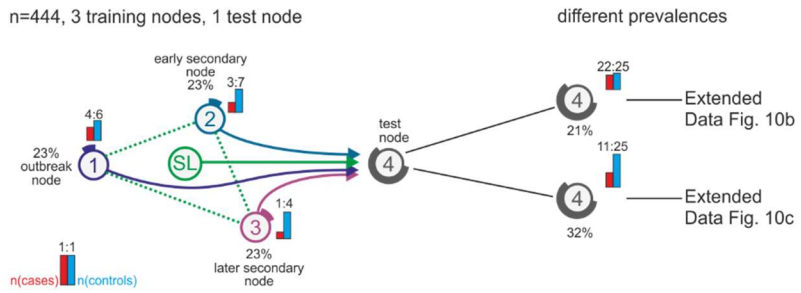

b

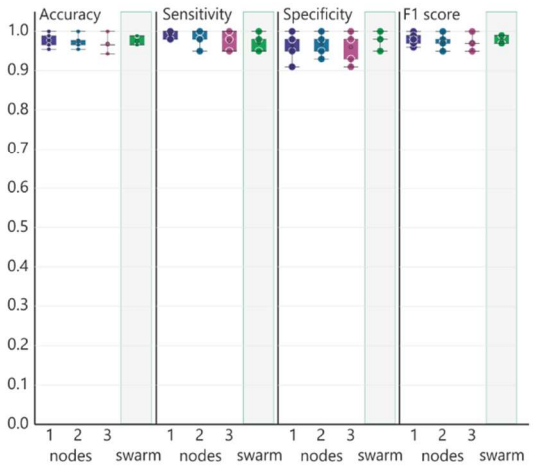

c

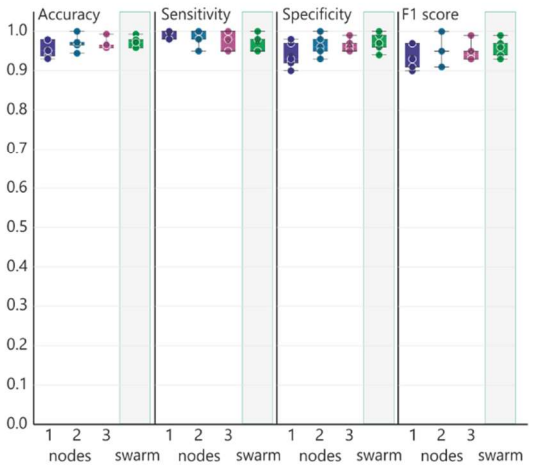

d

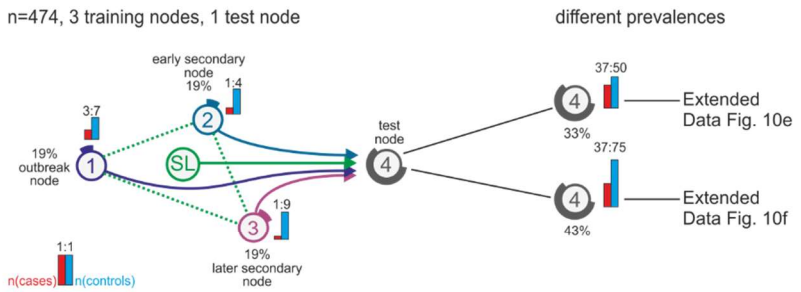

e

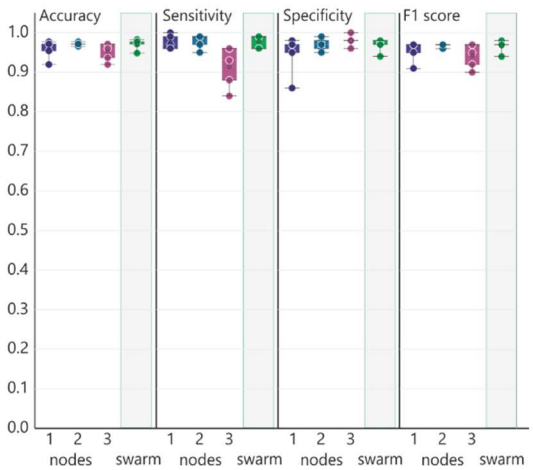

f

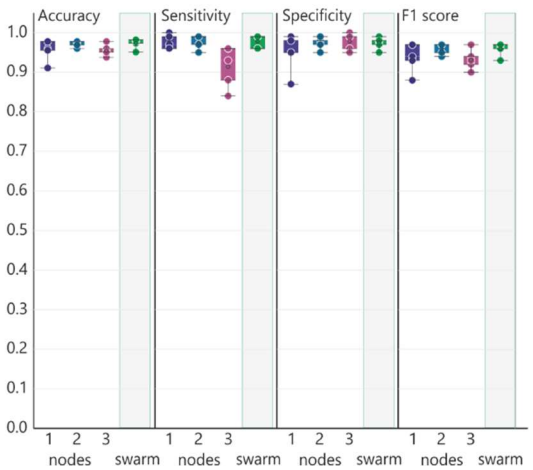

802

Extended Data Figure 10. Scenario with reduced prevalence at training nodes for detecting COVID-19 patients

(a) This scenario has the same sample size at each training node, but the prevalence decreases from node 1 to node 3. There are two different test sets (b) and (c). **(b)** Evaluation of scenario (a) with 22:25 ratio at the test node. **(c)** Results for the evaluation of scenario (a) with reduced prevalence. **(d)** Scenario similar to (a) but the prevalence has a steeper decrease between node 1 and 3. **(e)** Evaluation of scenario (d) with a ratio of 37:50 at the test node. **(f)** Evaluation of (d) with a reduced prevalence compared to (e). Box-whisker plot (mean, 1st and 3rd quartile, whisker type Min/Max). Statistical differences between results derived by SL and individual nodes including all permutations performed were calculated with Wilcoxon signed rank test with continuity correction; asterisk and line: $p<0.05$.

Extended Data Figure 11

a

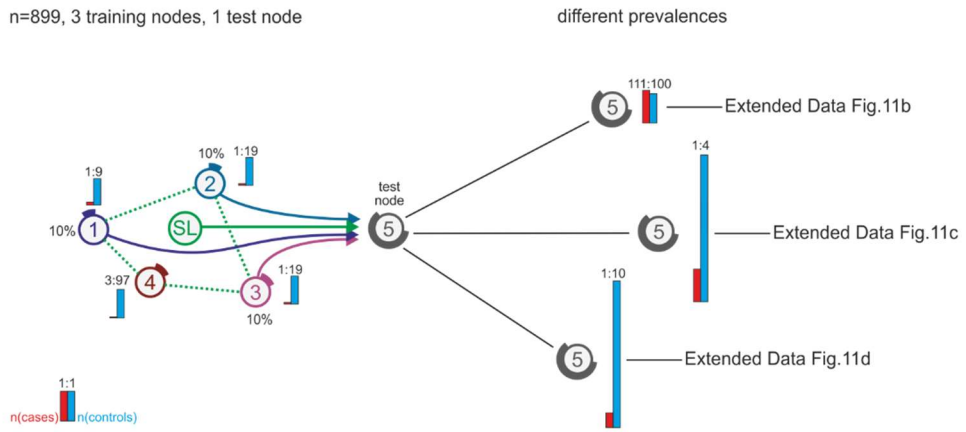

b

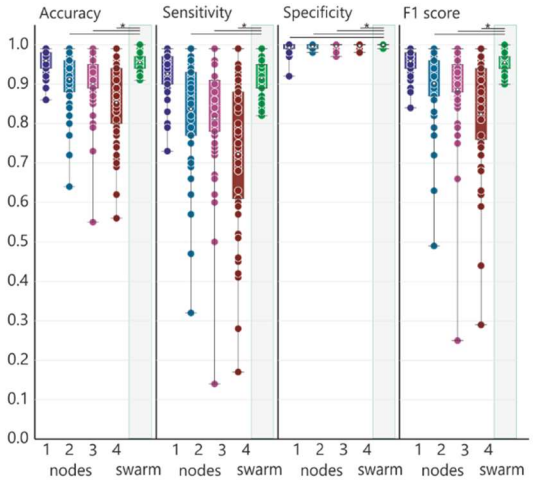

c

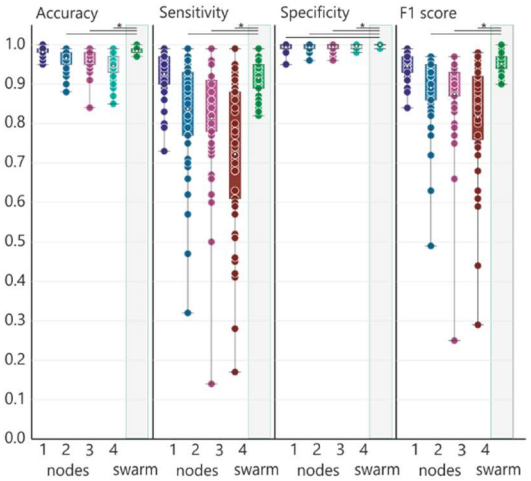

d

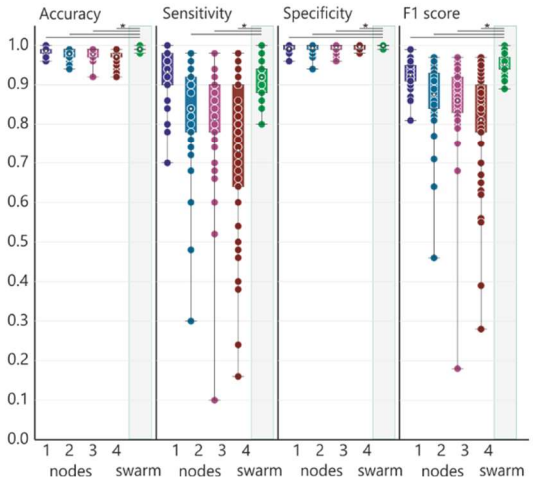

Extended Data Figure 11. Scenario with reduced prevalence in training and test set at a 4-node setting (a) This scenario has even training set sizes among the nodes with the prevalence ranging from 10% at node 1 to 3% at nodes 3 and 4. There are three different test sets (b), (c) and (d) with decreasing prevalence and increasing total sample size. **(b)** Evaluation of scenario (a) with 111:100 ratio. **(c)** Evaluation of scenario (a) with 1:4 ratio and increased sample number of the test set. **(d)** Results of scenario (a) with 1:10 prevalence and increased sample number of the test set. Box-whisker plot (mean, 1st and 3rd quartile, whisker type Min/Max). Statistical differences between results derived by SL and individual nodes including all permutations performed were calculated with Wilcoxon signed rank test with continuity correction; asterisk and line: $p<0.05$.

826 # Supplementary Information
827 # (Material and Methods)
828
829 ## Datasets

830 **Peripheral blood mononuclear cell (PBMC) derived transcriptome dataset (Dataset A)**

831 We used a previously described dataset containing over 12,000 transcriptomes derived from
832 peripheral blood mononuclear cells (PBMC), deposited at the National Center for
833 Biotechnology Information Gene Expression Omnibus[68] (GEO) under SuperSeries
834 GSE122517 or via the individual SubSeries GSE122505 (dataset 1), GSE122511 (dataset 2)
835 and GSE122515 (dataset 3). Briefly, this dataset was generated by inspection of all publicly
836 available datasets at GEO on September 20th, 2017. Inclusion criteria were cell type (PMBCs)
837 and species (*Homo sapiens*). Existing GEO SuperSeries were excluded to avoid duplicated
838 samples. According to data generation method, three datasets were established; dataset 1,
839 generated with Affymetrix HG-U133 A microarrays (n=2,500), dataset 2 with Affymetrix HG-
840 U133 2.0 microarrays (n=8,348), and dataset 3 with high-throughput RNA sequencing (RNA-
841 seq)(n=1,181). Data were curated as previously described[47]. All sample information is listed
842 in **Supplementary Table 2.**

843

844 **Whole blood derived transcriptomes for the prediction of tuberculosis (Dataset B)**

845 To establish a dataset based on whole blood transcriptomes we generated new data from
846 healthy controls (Rhineland Study) and combined these with previously generated data that
847 had been deposited in Gene Expression Omnibus (GEO). We screened for transcriptome
848 datasets derived from human whole blood samples, which were collected using the PAXgene
849 Blood RNA System. In total, nine independent datasets were selected to be included in the
850 present study (GSE101705 (n=44); GSE107104 (n=33), GSE112087 (n=120), GSE128078
851 (n=99), GSE66573 (n=14), GSE79362 (n=355), GSE84076 (n=36); GSE89403 (n=914)). The
852 newly generated 384 whole blood samples were sampled in context of the Rhineland Study
853 led by the German Center for Neurodegenerative Diseases (DZNE), which is an extensive
854 longitudinal study monitoring healthy individuals over 2 decades. Approval to undertake the
855 Rhineland Study was obtained from the ethics committee of the University of Bonn, Medical
856 Faculty. The study is carried out in accordance with the recommendations of the International
857 Conference on Harmonization (ICH) Good Clinical Practice (GCP) standards (ICH-GCP).
858 Written informed consent was obtained from all participants in accordance with the Declaration

859 of Helsinki. Overnight fasting blood was collected from all participants, including a PAXgene®
860 tube for RNA extraction and RNA-seq analysis. In total, Dataset B contained 1999 samples
861 from patients with active tuberculosis (n=775), latent tuberculosis (n=277), fatigue (n=55),
862 autoimmune diseases (n=68), HIV (n=16) and controls (n=808). Sample information is listed
863 in **Supplementary Table 2**.

864

865 **Whole blood derived transcriptome dataset for the prediction of COVID-19 (Dataset C)**

866

867 To develop classifiers based on whole blood transcriptomes able to predict COVID-19 patients
868 we collected an additional 134 PAXgene® tubes for RNA extraction and RNA-seq analysis
869 from COVID-19 patients, of which 93 whole blood samples at the Intensive Care Unit of the
870 Radboud University Medical Centre in Nijmegen, the Netherlands, and 41 samples were either
871 collected at the Sotiria Athens General Hospital or the ATTIKON University General Hospital
872 in Athens, Greece. For all COVID-19 patients, the study was carried out in accordance with
873 the applicable rules concerning the review of research ethics committees and informed
874 consent. All patients or legal representatives were informed about the study details and could
875 decline to participate. COVID-19 was diagnosed by a positive SARS-CoV-2 RT-PCR test in
876 nasopharyngeal or throat swabs and/or by typical chest CT-scan finding. Blood for RNA-seq
877 analysis was sampled on day 0 to 11 after admission. In the cohort in Athens, blood samples
878 from ten healthy donors who were tested negative on SARS-CoV-2 were included as controls.
879 The newly generated samples from the COVID-19 patients and the controls from Athens were
880 combined with dataset B (see above) to establish Dataset C. As a result, in addition to the
881 1999 samples derived from Dataset B, Dataset C included further 10 healthy controls and 134
882 dutch COVID-19 samples, which makes a total of 2,143 samples. Sample information is listed
883 in **Supplementary Tables 2 and 6**.

884

885 ## Pre-processing

886 **PBMC transcriptome dataset (Dataset A)**

887 We used a previously published dataset compiled for predicting AML in blood transcriptomes
888 derived from peripheral blood mononuclear cells (PBMC)[47]. Briefly, all raw data files were
889 downloaded from GEO and the RNA-seq data was preprocessed using the kallisto aligner
890 against the human reference genome gencode v27 (GRCh38.p10). For normalization, we
891 considered all platforms independently, meaning that normalization was performed separately
892 for the samples in Dataset A1, A2 and A3, respectively. Microarray data (Datasets A1 and A2)

893 was normalized using the robust multichip average (RMA) expression measures[69], as
894 implemented in the R package affy[70]. RNA-seq data (Dataset A3) was normalized with the R
895 package DESeq2 using standard parameters[71]. In order to keep the datasets comparable,
896 data was filtered for genes annotated in all three datasets, which resulted in 12,708 genes. No
897 filtering of low-expressed genes was performed. All scripts used in this study for pre-
898 processing are provided as a docker container on Docker Hub (docker hub,
899 https://hub.docker.com/r/schultzelab /aml_classifier).

900

901 **Whole blood derived transcriptome datasets (Datasets B and C)**

902 Since alignment of whole blood transcriptome data can be performed in numerous different
903 ways, we re-aligned all downloaded and collected datasets which were 4.7 Terabyte in size
904 and comprised a total of 7.8 Terabases, to the human reference genome gencode v33
905 (GRCh38.p13) and quantified transcript counts using STAR, an ultrafast universal RNA-seq
906 aligner (version 2.7.3a) [72]. For all samples in Datasets B and C, raw counts were imported
907 using DESeqDataSetFromMatrix function and size factors for normalization were calculated
908 using the DESeq function using standard parameters[71]**.** This was done separately for Dataset
909 B and Dataset C. Since some of the samples were prepared with poly-A selection to enrich
910 for protein-coding mRNAs, we filtered the complete dataset for protein-coding genes in order
911 to ensure greater comparability across library preparation protocols. Furthermore, we
912 excluded all ribosomal protein-coding genes, as well as mitochondrial genes and genes coding
913 for hemoglobins, which resulted in 18,135 transcripts as the feature space in Dataset B and
914 19,358 transcripts in Dataset C. Furthermore, transcripts with an overall expression < 10 were
915 excluded from further analysis. Other than that, no filtering of transcripts was performed. Prior
916 to use in machine learning we performed a rank transformation to normality on both datasets
917 B and C[73]. Briefly, transcript expression values were transformed from RNAseq counts to their
918 respective ranks. This was done transcript-wise, meaning all transcript expression values per
919 sample were given a rank based on ordering them from lowest to highest value. The rankings
920 were then turned into quantiles and transformed via the inverse cumulative distribution
921 function of the Normal distribution. This leads to all transcripts following the exact same
922 distribution (that is, a standard Normal with a mean of 0 and a standard deviation of 1) across
923 all samples

924 ## Methods details

925 **Scenarios for prediction of AML**

926 We previously demonstrated that ML on PBMC transcriptomes can be utilized to predict
927 AML[47]. Based on this experience, we generated sample sets within three independent
928 transcriptome datasets (dataset A1-A3, see above) to assess different scenarios in a three-
929 node setting for training with a fourth node only used for testing. As indicated in **Fig. 2**, six
930 scenarios with varying numbers of samples per node and varying ratios between cases and
931 controls at each node where defined. For predicting AML, all samples derived from AML
932 patients were classified as cases, while all other samples were labeled controls. When
933 predicting ALL, all samples derived from ALL patients were classified as cases and all others
934 as controls. For each scenario (**Fig. 2**) and each dataset we permuted the sample distribution
935 100 times, resulting in a total of 5,594 individual predictions. The different scenarios were
936 chosen to address the influence of sample numbers per node, the case control ratio, study
937 design-related batch effects, and transcriptome technologies used on classifier performance
938 at the nodes, but more importantly on swarm learning performance. Sample distributions for
939 all permutations within all scenarios are listed in **Supplementary Table 1**.

940

941 **Scenarios for detecting patients with acute TB**

942 In line with the experience we gained from the prediction of AML, we used dataset B to
943 generate scenarios for the prediction of tuberculosis in various settings, again using different
944 scenarios in a three-node setting for training with a fourth node only used for testing. In one
945 scenario, all patients with tuberculosis (Tb) including patients with latent and acute Tb were
946 treated as cases, while all others were defined as controls (**Extended Data Fig. 6b**). In all
947 other scenarios, cases were restricted to acute Tb patients' samples, while patients with latent
948 Tb were defined as controls together with all other non-Tb samples. Here, the question to be
949 answered is, whether the classifiers can identify patients with acute Tb and can distinguish
950 them from latent Tb and other conditions.

951 In one scenario (**Fig. 3c-d**), we added three additional training nodes to test dependency of
952 classifier performance by the number of nodes. As indicated in **Fig. 3**, three scenarios with
953 varying numbers of samples per node and varying ratios between cases and controls at each
954 node where defined. For scenarios described within **Fig. 3e,g** and **Fig. 3i,k**, we tested two
955 prevalence scenarios in the test set. For each scenario (**Fig. 3**) we permuted the sample
956 distribution 5-10 times, resulting in a total of 325 individual predictions. To mimic an outbreak
957 scenario, we reduced cases also at the training nodes to determine the effects on Swarm
958 Learning performance. Sample distributions for all permutations within all scenarios are listed
959 in **Supplementary Table 1**.

960

Simulation of an outbreak scenario to detect COVID-19 patients

Based on the promising results obtained with tuberculosis, we next intended to simulate classifier building and testing for the prediction of COVID-19 in a SL setting. We used dataset B and added 144 additional samples, of which 139 samples were derived from COVID-19 patients (see above). We applied a three-node setting for training with a fourth node only used for testing.

In one scenario (**Extended Data Fig. 8**), we kept cases (n=30) and controls (n=30) evenly distributed among the three training nodes and tested three different prevalence scenarios at the test node (22:25; 11:25; 1:44). In a second scenario (**Extended Data Fig. 9a-c**) we changed the ratio of cases and controls at each node (node 1: 40:60, node 2: 30:70, node 3: 20:80) and tested two prevalence scenarios at the test node (22:25; 11:25). In a third scenario (**Extended Data Fig. 9a-c**) we further reduced the number of cases at the training nodes further (node 1: 30:70, node 2: 20:80, node 3: 10:90) and tested two prevalence scenarios at the test node (37:50; 37:75).

Lastly, we tested an outbreak scenario (**Fig. 4**) with very few cases at the outbreak node 1 (20:80), an early secondary node (10:90) and a later secondary node (5:95) and three prevalence scenarios at the test node (1:1, 1:2, 1:10), resulting in a total of 220 individual predictions Sample distributions for all permutations within all scenarios are listed in **Supplementary Table 1**.

Application layer

The application layer (see also **Fig. 1g**) consists of disease models for which definitions are given, which samples are cases and which samples are controls. For example, if the classifier is supposed to detect all patients with tuberculosis (Tb), the model includes patients with latent and acute tuberculosis as cases and all other samples as controls. However, if only patients with acute tuberculosis are intended to be detected as cases, the model is changed in that cases are now only patient samples derived from patients with acute Tb, while samples from patients with latent Tb are now treated as controls, similar to all other non-Tb samples. The cases and controls used for each scenario are given in the result section in more detail. For each mode, classifiers are generated by applying neural networks (for description see below)

Computation and analysis

Neural network algorithm

We leveraged a deep neural network with a sequential architecture as implemented in the keras library (Keras, https://keras.io/, 2015). Briefly, the neural network consists of one input layer, eight hidden layers and one output layer. The input layer is densely connected and consists of 256 nodes, a rectified linear unit activation function and a dropout rate of 40%. From the first to the eighth hidden layer, nodes are reduced from 1024 to 64 nodes, and all layers contain a rectified linear unit activation function, a kernel regularization with an L2 regularization factor of 0.005 and a dropout rate of 30%. The output layer is densely connected and consists of 1 node and a sigmoid activation function. The model is configured for training with Adam optimization and to compute the binary cross-entropy loss between true labels and predicted labels.

The model has been translated from R to Python in order to make it compatible with the swarm learning library. This model is used for training both the individual nodes as well as swarm learning. The model is trained over 100 epochs, with varying batch sizes. The batch size of 8, 16, 32, 64 and 128 are used depending on the number of training samples.

Preparation and adaptation of neural network code to be used in a swarm learning environment

A swarm callback is introduced to integrate the model with the Swarm Learning library. Minimum number of nodes for synchronization, synchronization interval, validation dataset and batch size are passed as parameters to swarm callback. The swarm call back API is

```
swCallback = SwarmCallback( sync_interval =  <number of training batches between syncs>,
                            min_peers = <minimum peers>,
                            val_data = <validation dataset>,
                            val_batch_size = <validation batch size>,
                            node_weightage = <relative weightage of node's model weights>)
```

sync_interval specifies the synchronization interval,

min_peers specifies the minimum number of nodes for model synchronization,

val_data specifies the validation data set,

val_batch_size specifies the validation batch size,

model_name specifies the name of the model,

node_weightage specifies the relative weightage to be given to model weights of this node

Parameter tuning

For some of the scenarios we tuned model hyperparameters. For some scenarios we also tuned Swarm Learning parameters to get better performance, for example higher sensitivity.

For AML **Fig. 2e**, **Extended Data Fig. 2** and **Fig. 2f**, dropout rate is reduced to 10% to get better performance. For AML **Fig. 2b**, **Extended Data Fig. 1**, dropout rate is reduced to 10% and increased the Epochs to 300 to get better performance. We also used the adaptive_rv parameter in the Swarm Learning API to adjust the merge frequency dynamically based on model convergence to improve the training time. For TB and COVID-19 tests dropout rate is reduced to 10% for all scenarios. For the TB scenarios in **Extended Data Fig. 7a,b**, the node_weightage parameter of Swarm Learning callback API is used to give more weightage to the nodes that have higher case samples.

Infrastructure layer

Description of the hardware architecture applied for simulations

For all simulations provided in this project we used 2 HPE Apollo 6500 Gen 10 server, each with 4 Intel(R) Xeon(R) CPU E5-2698 v4 @ 2.20GHz, a 3.2 TB hard disk drive, 256 GB RAM, 8 Tesla P100 GPUs, 1GB network interface card for LAN access and infiniBand FDR for high speed interconnect and networked storage access. The Swarm Network is created with 3 nodes, each node is a docker container with 1 GPU. Multiple experiments were run in parallel using the above described configuration.

Overall, we performed 6,139 analyses including six scenarios for all three AML datasets, nine scenarios for Tb and 10 scenarios for COVID-19. We performed 5 to 100 permutations per scenario, each permutation took approximately 30 minutes, which resulted in a total of 3069,5 compute hours.

The Swarm learning framework, library, distributed ML and blockchain technologies

Swarm Learning builds on top of two proven technologies — distributed ML and blockchain. Distributed ML is leveraged to train a common model across multiple nodes with a subset of the data located at each node — commonly known as the data parallel paradigm in ML — though without a central parameter server. Blockchain lends the decentralized control, scalability, and fault-tolerance aspects to the Swarm Network system to enable the framework to work beyond the confines of a single enterprise.

The Swarm Learning library is a framework to enable decentralized training of ML models without sharing the data. The Swarm Learning framework is designed to make it possible for a set of nodes — each node possessing some training data locally — to train a common ML

model collaboratively without sharing the training data itself. This can be achieved by individual nodes sharing parameters (weights) derived from training the model on the local data. This allows nodes to maintain the privacy of their raw data. Importantly, in contrast to many existing federated learning models, a central parameter server is omitted in Swarm Learning.

The nodes that participate in Swarm Learning, register themselves with the Swarm Network implicitly using the callback API. Here, the Swarm Network interacts with other peers using blockchain for sharing parameters and for controlling the training process. On each node, a simple Swarm callback API has to be used to enable the ML model with Swarm Learning capacities (see also code presented below). The Swarm container has to be configured to interact with the Swarm Network (network i/p and port configuration). All other complexities of setting up network, registration, parameter sharing, and parameter merging are taken care of by the Swarm callback API and the Swarm Network infrastructure.

Parameters shared from all the nodes are merged to obtain a global model. Moreover, the merge process is not done by a static central coordinator or parameter server, but rather a temporary leader chosen dynamically among the nodes is used to perform the merge, thereby making the Swarm network decentralized. This provides a far greater fault-tolerance than traditional centralized-parameter-server-based frameworks. All the nodes can perform the role of training and merging, thereby maximising the usage of local compute. The Swarm Network implicitly controls this.

The HPE Swarm Learning library contains 2 containers, the Swarm Network container and the Swarm ML container.

The Swarm Network container includes 1) software to setup and initialize the Swarm Network, 2) management commands to control the Swarm Network, and 3) start/stop Swarm Learning tasks. This container also encapsulates the blockchain software.

The Swarm ML container includes software to support 1) decentralized training, 2) integration with ML frameworks, and 3) it exposes APIs for ML models to interact with Swarm Learning.

For any ML model to be applied to Swarm Learning, it needs to be modified using the Swarm callback API. The callback API provides options to control the Swarm Learning processes. To convert a ML program into a Swarm ML program the following steps have to be performed:

1. Import the SwarmCallback class from the swarm library

```
from swarm ‘import SwarmCallback’
```

SwarmCallback is a custom callback class that is built on the Keras Callback class.

2. Instantiate an object of the SwarmCallback class:

```
swarm_callback = SwarmCallback(   min_peers = <peer count>,
                                  sync_interval = <interval>,
                                  use_adaptive_sync = <bool>,
                                  val_batch_size = <batch size>,
                                  val_data = <either a (x_val, y_val) tuple or a
                                              generator>
                                  node_weightage = <relative weightage of node's
                                model weights> ).
```

In this context, 'min_peers' specifies the minimum number of network peers required to synchronize the insights, 'sync_interval' specifies the number of batches after which a synchronization is performed, 'use_adaptive_sync' specifies whether the *adaptive sync interval* feature should be used for tuning the sync interval. This feature is turned off by default; ' val_batch_size' specifies the size of each validation batch; 'val_data' specifies the validation dataset. It can be either a (x_val, y_val) tuple or a generator;

3. Pass the object to the list of callbacks in Keras training code: model.fit(..., callbacks = [swarm_callback]). SwarmCallback can be included along with other callbacks also:

```
es_callback = EarlyStopping(...);
model.fit(..., callbacks = [es_callback, swarm_callback])
```

The Swarm Learning architecture principles

The Swarm Learning framework has two major components, 1) the Swarm ML component runs a user-defined Machine Learning algorithm, and 2) the Swarm Network component forms the Swarm Network based on a blockchain network.

The Swarm ML component is implemented as an API available for multiple popular frameworks such as TensorFlow, Keras, Pytorch. This API provides an interface that is similar to the training APIs in the native frameworks familiar to data scientists. Calling this API automatically inserts the required hooks for Swarm Learning so that nodes seamlessly exchange parameters and subsequently continue the training after setting the local models to the globally merged parameters. With a few simple code changes, the entire network learns as one cohort, with all the complexities of control and data flow taking place in an automated fashion.

Within the Swarm Network component each Swarm ML component interacts with each other using the Swarm Network component's blockchain platform to maintain global state information about the model that is being trained and to track the training progress. The Swarm Network components use this state and progress information to coordinate the working of the Swarm learning. The Swarm Network is responsible for keeping the decentralized Swarm network in a globally consistent state. The Swarm Network ensures that all operations and the corresponding state transitions are performed in a synchronous manner. Both, state and supported operations of the system are encapsulated in a blockchain smart contract. The Swarm Network contains the logic to elect the leader of the Swarm for every synchronization, implement fault-tolerance, and self-healing mechanisms, along with signaling among nodes for commencement and completion of various phases.

The Swarm Learning framework is designed to run on both commodity and high-end machines, supporting a heterogeneous set of infrastructure in the network. It can be deployed within and across data centers.

In contrast to federated learning with star topology and a centralized coordinator, Swarm Learning can support multiple topologies including fully connected, mesh, star, tree and hybrid topologies. This flexibility provides multiple options to cater into different use cases.

The Swarm Learning process

Swarm Learning provides a callback API to enable swift integration with multiple frameworks. This API is incorporated into the existing ML code to quickly transform a stand-alone ML node into a Swarm Learning participant in a non-intrusive way. It offers a set of commands (APIs) to manage the Swarm Network and control the training.

The Swarm learning process is as follows:

The Swarm Learning process begins with enrollment of nodes with Swarm Network, which is done implicitly by Swarm callback function when the callback is constructed. During this process, the relevant attributes of the node are stored in the blockchain ledger. This is a one-time process.

Nodes will train the local copy of the model iteratively using private data over multiple epochs. During each epoch, the node trains its local model using one or more data batches for a fixed number of iterations. It regularly shares its learnings with the other Swarm nodes and incorporates their insights. Users can control the periodicity of this sharing by defining a

Synchronization Interval in Swarm callback API. This interval specifies the number of training batches after which the nodes will share their learnings.

At the end of every synchronization interval, when it is time to share the learnings from the individual models, one of the Swarm nodes is elected as a "leader" using the leader election logic. This leader node collects the model parameters from each peer node and merges them. The framework supports multiple merge algorithms such as mean, weighted mean, median, and so on. Each node then uses these merged parameters to calculate various validation metrics. These results are compared against the stopping criterion and if it is found to be met, the Swarm Learning process is halted. Else the nodes use the merged parameters to start the next training batch.

Swarm Learning library uses blockchain smart contracts to define the leader election logic and the merge algorithm. The blockchain smart contracts prevents attacks from semi-honest or dishonest participants.

Quantification and Statistical Analysis

We evaluated binary classification model performance with sensitivity, specificity, accuracy and f1-score metrics. Sensitivity, specificity, accuracy and f1-score were determined for every test run. The 95% confidence intervals of all performance metrices were estimated using the boostrapping approach[74]. For AML and ALL, 100 permutations per scenario were run for each scenario. For TB the performance metrics were collected by running 10 permutations for scenarios 1 to 4 and 5 permutations for scenarios 5 to 10. For COVID-19 the performance metrics were collected by running 20 permutations for each scenario. All metrics are listed in **Supplementary Tables 3 and 4.**

Differences in performance metrics were tested using the Wilcoxon signed rank test with continuity correction (Individual Comparisons by Ranking Methods, Frank Wilcoxon, https://sci2s.ugr.es/keel/pdf/algorithm/articulo/wilcoxon1945.pdf). All test results are provided in **Supplementary Table 5**.

To run the experiments, we used Python version 3.6.9 with Keras version 2.3.1 and Tensorflow version 2.2.0-rc2. We used scikit-learn library version 0.23.1[75] to calculate values for the metrics. Summary statistics and hypothesis tests were calculated using R version 3.5.2 (R: A language and environment for statistical computing, http://www.R-project.org/., 2015). Calculation of each metric was done as follows:

$$Sensitivity = \frac{TP}{TP + FN}$$

$$Specificity = \frac{TN}{TN + FP}$$

$$Accuracy = \frac{TP + TN}{TP + FP + TN + FN}$$

$$Balanced\ Accuracy = \frac{Sensitivity + Specificity}{2}$$

$$F1 - score = \frac{2TP}{FP + FN + 2TP}$$

where TP=True Positive, FP=False Positive, TN=True Negative, FN=False Negative

Data visualization

The classification report and confusion matrix was generated with scikit-learn APIs for each permutation. Measurements of sensitivity, specificity and accuracy of each permutation run was read into a table in Excel using Power Query and used for visualization for the different scenarios in Power BI [Version: 2.81.5831.821 64-bit (Mai 2020)] with Box and Whisker chart by MAQ Software (https://appsource.microsoft.com/en-us/product/power-bi-visuals/WA104381351).

Data and software availability:

Processed data can be accessed via the SuperSeries GSE122517 or via the individual SubSeries GSE122505 (dataset A1), GSE122511 (dataset A2) and GSE122515 (dataset A3). Dataset B consists of the following series which can be accessed at GEO: GSE101705, GSE107104, GSE112087, GSE128078, GSE66573, GSE79362, GSE84076, and GSE89403. Furthermore, it contains the Rhineland study. This dataset is not publicly available because of data protection regulations. Access to data can be provided to scientists in accordance with the Rhineland Study's Data Use and Access Policy. Requests for further information or to access the Rhineland Study's dataset should be directed to RS-DUAC@dzne.de. Dataset C contains dataset B and additional samples for COVID-19. These datasets are made available at the European Genome-Phenome Archive (EGA) under accession number EGAS00001004502, which is hosted by the EBI and the CRG.

The code for preprocessing and for predictions can be found at GitHub (https://github.com/schultzelab/swarm_learning).

Supplementary Tables

Supplementary Table 1:	Overview over all sample numbers and scenarios
Supplementary Table 2:	Dataset annotations of Dataset A, B and C
Supplementary Table 3:	Prediction results for all scenarios and permutations
Supplementary Table 4:	Summary statistics on all prediction scenarios
Supplementary Table 5:	Statistical tests comparing single node vs. swarm predictions
Supplementary Table 6:	Covid 19 Patient characteristics

References

1. Haendel, M. A., Chute, C. G. & Robinson, P. N. Classification, ontology, and precision medicine. *N. Engl. J. Med.* **379**, 1452–1462 (2018).
2. Aronson, S. J. & Rehm, H. L. Building the foundation for genomics in precision medicine. *Nature* **526**, 336–342 (2015).
3. Courtiol, P. *et al.* Deep learning-based classification of mesothelioma improves prediction of patient outcome. *Nat. Med.* **25**, 1519–1525 (2019).
4. Liang, H. *et al.* Evaluation and accurate diagnoses of pediatric diseases using artificial intelligence. *Nat. Med.* **25**, 433–438 (2019).
5. Wiens, J. *et al.* Do no harm: a roadmap for responsible machine learning for health care. *Nat. Med.* **25**, (2019).
6. He, J. *et al.* The practical implementation of artificial intelligence technologies in medicine. *Nat. Med*. **25**, 30–36 (2019).
7. Babic, B., Gerke, S., Evgeniou, T. & Glenn Cohen, I. Algorithms on regulatory lockdown in medicine. *Science* **366**, 1202–1204 (2019).
8. Price, W. N. & Cohen, I. G. Privacy in the age of medical big data. *Nat. Med*. **25**, 37–43 (2019).
9. Zhang, X. *et al.* Viral and host factors related to the clinical outcome of COVID-19. *Nature* (2020) doi:10.1038/s41586-020-2355-0.
10. Berlin, D. A., Gulick, R. M. & Martinez, F. J. Severe Covid-19. *N. Engl. J. Med.* (2020) doi:10.1056/nejmcp2009575.
11. Gandhi, R. T., Lynch, J. B. & del Rio, C. Mild or Moderate Covid-19. *N. Engl. J. Med.* (2020) doi:10.1056/nejmcp2009249.
12. Cho, A. AI systems aim to sniff out coronavirus outbreaks. *Science* **368**, 810–811 (2020).
13. Peiffer-Smadja, N. *et al.* Machine Learning for COVID-19 needs global collaboration and data-sharing. *Nat. Mach. Intell.* 1–2 (2020) doi:10.1038/s42256-020-0181-6.
14. Luengo-Oroz, M. *et al.* Artificial intelligence cooperation to support the global response to COVID-19. *Nat. Mach. Intell.* 1–3 (2020) doi:10.1038/s42256-020-0184-3.
15. Hu, Y. *et al.* The challenges of deploying artificial intelligence models in a rapidly evolving pandemic. *Nat. Mach. Intell.* **2**, 298–300 (2020).
16. Senior, A. W. *et al.* Improved protein structure prediction using potentials from deep learning. *Nature* **577**, 706–710 (2020).
17. Ge, Y. *et al.* A data-driven drug repositioning framework discovered a potential therapeutic agent targeting COVID-19. *bioRxiv* (2020) doi:10.1101/2020.03.11.986836.
18. Ting, D. S. W., Carin, L., Dzau, V. & Wong, T. Y. Digital technology and COVID-19. *Nat. Med*. **26**, 459–461 (2020).
19. Cohen, I. G., Gostin, L. O. & Weitzner, D. J. Digital Smartphone Tracking for COVID-19: Public Health and Civil Liberties in Tension. *JAMA* (2020) doi:10.1001/jama.2020.8570.
20. Jia, J. S. *et al.* Population flow drives spatio-temporal distribution of COVID-19 in China. *Nature* (2020) doi:10.1038/s41586-020-2284-y.
21. Mei, X. *et al.* Artificial intelligence-enabled rapid diagnosis of patients with COVID-19. *Nat. Med.* (2020) doi:10.1038/s41591-020-0931-3.

22. Zhang, K. *et al.* Clinically Applicable AI System for Accurate Diagnosis, Quantitative Measurements, and Prognosis of COVID-19 Pneumonia Using Computed Tomography. *Cell* **181**, (2020).

23. Amisha, Malik, P., Pathania, M. & Rathaur, V. Overview of artificial intelligence in medicine. *J. Fam. Med. Prim. Care* **8**, 2328 (2019).

24. Hosny, A., Parmar, C., Quackenbush, J., Schwartz, L. H. & Aerts, H. J. W. L. Artificial intelligence in radiology. *Nature Reviews Cancer*. **18**, 500–510 (2018).

25. Lecun, Y., Bengio, Y. & Hinton, G. Deep learning. *Nature*. **521**, 436–444 (2015).

26. Kaissis, G. A., Makowski, M. R., Rückert, D. & Braren, R. F. Secure, privacy-preserving and federated machine learning in medical imaging. *Nat. Mach. Intell.* (2020) doi:10.1038/s42256-020-0186-1.

27. Rajkomar, A., Dean, J. & Kohane, I. Machine learning in medicine. *New England Journal of Medicine* vol. 380 1347–1358 (2019).

28. Obermeyer, Z. & Emanuel, E. J. Predicting the future-big data, machine learning, and clinical medicine. *New England Journal of Medicine*. **375**, 1216–1219 (2016).

29. Savage, N. Machine learning: Calculating disease. *Nature*. **550**, S115–S117 (2017).

30. Ping, P., Hermjakob, H., Polson, J. S., Benos, P. V. & Wang, W. Biomedical informatics on the cloud: A treasure hunt for advancing cardiovascular medicine. *Circ. Res.* **122**, 1290–1301 (2018).

31. Chouvarda, I. *et al.* WELCOME - Innovative integrated care platform using wearable sensing and smart cloud computing for COPD patients with Comorbidities. in *2014 36th Annual International Conference of the IEEE Engineering in Medicine and Biology Society, EMBC 2014* vol. 2014 3180–3183 (Institute of Electrical and Electronics Engineers Inc., 2014).

32. Grossman, R. L. & White, K. P. A vision for a biomedical cloud. in *Journal of Internal Medicine*. **271**, 122–130 (J Intern Med, 2012).

33. Char, D. S., Shah, N. H. & Magnus, D. Implementing machine learning in health care ' addressing ethical challenges. *New England Journal of Medicine*. **378**, 981–983 (2018).

34. Gibney, E. The battle for ethical AI at the world's biggest machine-learning conference. *Nature*. **577**, 609 (2020).

35. Finlayson, S. G. *et al.* Adversarial attacks on medical machine learning. *Science.* **363**, 1287–1289 (2019).

36. Ienca, M. & Vayena, E. On the responsible use of digital data to tackle the COVID-19 pandemic. *Nat. Med*. **26**, 463–464 (2020).

37. Konečný, J., McMahan, H. B., Ramage, D. & Richtárik, P. Federated Optimization: Distributed Machine Learning for On-Device Intelligence. (2016).

38. Konečný, J. *et al.* Federated Learning: Strategies for Improving Communication Efficiency. (2016).

39. McMahan, H. B., Moore, E., Ramage, D., Hampson, S. & Arcas, B. A. y. Communication-Efficient Learning of Deep Networks from Decentralized Data. *Proc. 20th Int. Conf. Artif. Intell. Stat. AISTATS 2017* (2016).

40. Shokri, R. & Shmatikov, V. Privacy-Preserving Deep Learning | Proceedings of the 22nd ACM SIGSAC Conference on Computer and Communications Security. *ACM Digit. Libr.* 1310–1321 (2015).

41. Pathak, M., Rane, S., Sun, W. & Raj, B. Privacy preserving probabilistic inference with Hidden Markov Models. in *ICASSP, IEEE International Conference on Acoustics,*

Speech and Signal Processing - Proceedings 5868–5871 (2011). doi:10.1109/ICASSP.2011.5947696.

42. Chaussabel, D., Pascual, V. & Banchereau, J. Assessing the human immune system through blood transcriptomics. *BMC Biology*. **8**, (2010).

43. Chaussabel, D. Assessment of immune status using blood transcriptomics and potential implications for global health. *Seminars in Immunology*. **27**, 58–66 (2015).

44. Wei, Z. *et al.* Large sample size, wide variant spectrum, and advanced machine-learning technique boost risk prediction for inflammatory bowel disease. *Am. J. Hum. Genet.* **92**, 1008–1012 (2013).

45. Stephens, Z. D. *et al.* Big data: Astronomical or genomical? *PLoS Biol.* **13**, (2015).

46. Dove, E. S. *et al.* Genomic cloud computing: Legal and ethical points to consider. *Eur. J. Hum. Genet.* **23**, 1271–1278 (2015).

47. Warnat-Herresthal, S. *et al.* Scalable Prediction of Acute Myeloid Leukemia Using High-Dimensional Machine Learning and Blood Transcriptomics. *iScience* **23**, (2020).

48. Zak, D. E. *et al.* A blood RNA signature for tuberculosis disease risk: a prospective cohort study. *Lancet* **387**, 2312–2322 (2016).

49. Leong, S. *et al.* Existing blood transcriptional classifiers accurately discriminate active tuberculosis from latent infection in individuals from south India. *Tuberculosis* **109**, 41–51 (2018).

50. de Araujo, L. S. *et al.* Transcriptomic biomarkers for tuberculosis: Evaluation of DOCK9, EPHA4, and NPC2 mRNA expression in peripheral blood. *Front. Microbiol.* **7**, (2016).

51. Verma, S. *et al.* 'Tuberculosis in advanced HIV infection is associated with increased expression of IFNγ and its downstream targets'. *BMC Infect. Dis.* **18**, (2018).

52. Thompson, E. G. *et al.* Host blood RNA signatures predict the outcome of tuberculosis treatment. *Tuberculosis* **107**, 48–58 (2017).

53. Corman, V. M. *et al.* Detection of 2019 novel coronavirus (2019-nCoV) by real-time RT-PCR. *Eurosurveillance* **25**, (2020).

54. Schulte-Schrepping, J. *et al.* Suppressive myeloid cells are a hallmark of severe COVID-19. *medRxiv* 2020.06.03.20119818 (2020) doi:10.1101/2020.06.03.20119818.

55. McKinney, S. M. *et al.* International evaluation of an AI system for breast cancer screening. *Nature* **577**, 89–94 (2020).

56. Kermany, D. S. *et al.* Identifying Medical Diagnoses and Treatable Diseases by Image-Based Deep Learning. *Cell* **172**, 1122-1131.e9 (2018).

57. Ardila, D. *et al.* End-to-end lung cancer screening with three-dimensional deep learning on low-dose chest computed tomography. *Nat. Med.* **25**, 954–961 (2019).

58. Esteva, A. *et al.* Dermatologist-level classification of skin cancer with deep neural networks. *Nature* **542**, 115–118 (2017).

59. Kaissis, G. *et al.* A machine learning model for the prediction of survival and tumor subtype in pancreatic ductal adenocarcinoma from preoperative diffusion-weighted imaging. *Eur. Radiol. Exp.* **3**, (2019).

60. Kaissis, G. *et al.* A machine learning algorithm predicts molecular subtypes in pancreatic ductal adenocarcinoma with differential response to gemcitabine-based versus FOLFIRINOX chemotherapy. *PLoS One* **14**, (2019).

61. Cui, E. *et al.* Predicting the ISUP grade of clear cell renal cell carcinoma with multiparametric MR and multiphase CT radiomics. *Eur. Radiol.* **30**, 2912–2921 (2020).

62. Lu, H. *et al.* A mathematical-descriptor of tumor-mesoscopic-structure from computed-tomography images annotates prognostic- and molecular-phenotypes of epithelial ovarian cancer. *Nat. Commun.* **10**, (2019).

63. Elshafeey, N. *et al.* Multicenter study demonstrates radiomic features derived from magnetic resonance perfusion images identify pseudoprogression in glioblastoma. *Nat. Commun.* **10**, (2019).

64. Ryffel, T., Dufour-Sans, E., Gay, R., Bach, F. & Pointcheval, D. Partially Encrypted Machine Learning using Functional Encryption. (2019).

65. Salem, M., Taheri, S. & Yuan, J.-S. Utilizing Transfer Learning and Homomorphic Encryption in a Privacy Preserving and Secure Biometric Recognition System. *Computers* **8**, 3 (2018).

66. Dahl, M. *et al.* Private Machine Learning in TensorFlow using Secure Computation. (2018).

67. Shi, W. *et al.* Deep Learning-Based Quantitative Computed Tomography Model in Predicting the Severity of COVID-19: A Retrospective Study in 196 Patients. *SSRN Electron. J.* (2020) doi:10.2139/ssrn.3546089.

68. Edgar, R., Domrachev, M. & Lash, A. E. Gene Expression Omnibus: NCBI gene expression and hybridization array data repository. *Nucleic Acids Res.* (2002) doi:10.1093/nar/30.1.207.

69. Irizarry R. A. Exploration, Normalization, and Summaries of High Density Oligonucleotide Array Probe Level Data. *Biostatistics* (2003).

70. Gautier L. Affy--Analysis of Affymetrix GeneChip Data at the Probe Level. *Bioinformatiks* (2004).

71. Love, M. I., Huber, W. & Anders, S. Moderated estimation of fold change and dispersion for RNA-seq data with DESeq2. *Genome Biol.* **15**, (2014).

72. Dobin, A. *et al.* STAR: Ultrafast universal RNA-seq aligner. *Bioinformatics* **29**, 15–21 (2013).

73. Zwiener, I., Frisch, B. & Binder, H. Transforming RNA-Seq data to improve the performance of prognostic gene signatures. *PLoS One* **9**, (2014).

74. Efron, B. Bootstrap Methods: Another Look at the Jackknife. *Ann. Stat.* **7**, 1–26 (1979).

75. Pedregosa, F. *et al. Scikit-learn: Machine Learning in Python. Journal of Machine Learning Research*. **12**, (2011).